



Obstacle-avoidance trajectory planning based adaptive tracking control for 4DOF tower cranes with tracking error constraints

Wei Peng ^a, Hui Guo ^a, Menghua Zhang ^{b,*}, Chengdong Li ^{a,*}, Fang Shang ^a, Zhi Li ^a

^a The School of Information and Electrical Engineering, Shandong Jianzhu University, Jinan 250101, China

^b The School of Electrical Engineering, University of Jinan, Jinan 250022, China

ARTICLE INFO

Keywords:

Tower crane
Trajectory planning
Fuzzy neural network
Obstacle avoidance
Adaptive control

ABSTRACT

Due to the tower cranes usually working in an outdoor environment, it is generally unavoidable for the obstacle to exist in the transportation path. Thus, it is critical for the tower crane systems to guarantee their safety and efficiency simultaneously. In this paper, for the 4DOF tower cranes, a novel adaptive tracking control approach is proposed by considering obstacle-avoidance trajectory planning. The state constraint equations are established firstly, by involving the auxiliary terms. And, the optimal time trajectory with physical constraints is obtained by the dichotomy method. Then, the fuzzy neural network is employed to handle the obstacle-avoidance trajectories generation problem under the different final positions and obstacle positions. An adaptive tracking control method with error constraints is further given to guarantee the precise tracking of the trolley and the jib. It is noteworthy that the proposed method not only constrains the state variables within predefined ranges but also constructs an improved trajectory planning method for the first time to avoid collisions. Additionally, the stability of the system is theoretically proven by the Lyapunov technique and LaSalle's invariance principle. Finally, several experimental results demonstrate the superiority of the proposed method over comparative approaches in terms of effectiveness and robustness.

1. Introduction

With the fast development of the construction, especially the smart construction scenario, the tower cranes have become one kind of the most important building machineries [1,2]. Since the open and complex working environment, achieving the non-collisions and efficient operation is critical for the tower cranes [3–5]. On the other hand, as a typical underactuated system, the tower cranes exhibit distinctive dynamic characteristics, such as nonlinearity, strong coupling, and unactuation, etc. Therefore, it is challenging but necessary to propose an efficient tracking controller for achieving safe and efficient operation.

Over the past decades or so, many methods, including adaptive methods [6–8], sliding mode control [9–11], fuzzy control [12–14], and backstepping control [15,16], etc., have been proposed for achieving the objectives of precise positioning and anti-swing. Benefiting from the powerful uncertainties handling ability, various neural networks have attracted a great deal of attention. For instance, Zhang et al. proposed an Radial Basis Function Neural Network (RBFNN) based adaptive controller to handle uncertain parameters, external disturbances, and nonlinearity in [17]. In [18], authors introduced a Bayesian Regularized Artificial Neural Network (BRANN) to dynamically update shaper parameters based on the system's current parameters. Some research reflected that

* Corresponding authors.

E-mail addresses: zhangmenghua@mail.sdu.edu.cn (M. Zhang), lichengdong@sdjzu.edu.cn (C. Li).

the control methods considering constraints usually obtained better dynamic performances. In [19], authors designed the auxiliary terms to strengthen the couplings between unactuated and actuated states, based on which, the controller with the constraints of unactuated states was further proposed to tackle the positioning and anti-swing control. In [20] and [21], the tracking control with state constraints was devised to solve the motion control of the tower cranes under the actual physical constraints.

Although the above mentioned methods can bring proper control performance for the tower crane systems, there are few works concentrated on the obstacle avoidance problem. In [22], the payload path was pre-planned by considering the speeds of trolley translation and jib rotation, and then the obstacle avoidance controller was designed. In [23] and [24], the authors respectively proposed time-optimal trajectory planning methods for double-pendulum and rotary crane systems. As the aforementioned work, the obstacle was usually approximated as a single point, while neglecting its volumetric nature. In real-word, the volume of obstacles is hard to neglect, especially in the opening and complex construction scenario. And, the volume of obstacles will greatly affect the trajectory planning results and the tracking control performance. Hence, the obstacle-avoidance trajectory planning-based adaptive tracking control for the tower crane is worthy to further study.

Based on the above analysis, this paper proposes a novel adaptive control method with a time-optimal trajectory planning and tracking error constraints. The proposed method can guarantee the system to generate and follow an obstacle-avoidance trajectory, ultimately reaching a predetermined target. The main innovations and contributions can be summarized as follows:

- In order to effectively deal with the obstacle avoidance problem, new auxiliary terms are introduced to handle the actuated and the unactuated states, based on which, improved state equations are established considering the obstacle-avoidance and tracking error constraints.
- A novel adaptive tracking control approach is proposed by considering the obstacle-avoidance trajectory planning and tracking error constraints. The optimal time trajectory which considers the position and volume of the obstacle is accurately predicted by combining the dichotomy method with the Fuzzy Neural Network (FNN) together.
- To ensure tracking performance, predefined safe boundaries are given and adaptive laws are employed to estimate uncertain/unknown parameters. Then, the stability of the system is theoretically proven by the Lyapunov technique and LaSalle's invariance principle. Finally, several experimental results demonstrate the superiority of the proposed method over comparative approaches in terms of effectiveness and robustness.

The remainder of the paper is organized as follows: Section 2 gives the dynamic model of the 4-DOF tower. In Section 3, the obstacle avoidance trajectory is presented with variable constraints, which includes auxiliary signals design, time optimal trajectory planning, and FNN prediction design. Section 4 introduces the tracking controller with tracking error limitations, and analyzes the stability of the system. In Section 5, the experiments are provided and analyzed, which verifies the effectiveness of the control strategy. Lastly, some conclusions are given in Section 6.

2. Problem Statement

2.1. 4DOF tower crane dynamic model

By utilizing the Lagrangian modeling technique, the dynamic equation of 4DOF tower cranes can be expressed in the following matrix–vector form:

$$M(\mathbf{q})\ddot{\mathbf{q}} + C(\mathbf{q}, \dot{\mathbf{q}})\dot{\mathbf{q}} + G(\mathbf{q}) = \mathbf{U} - \mathbf{Uf}, \quad (1)$$

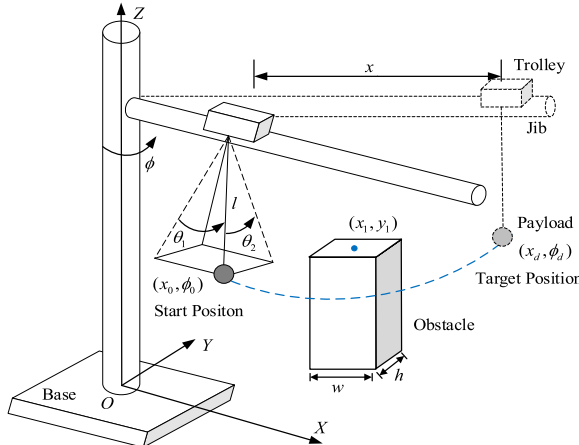


Fig. 1. Tower crane model with an obstacle.

where $\mathbf{q} = [\phi \ x \ \theta_1 \ \theta_2]^T$, $\mathbf{U} = [u_\phi \ u_x \ 0 \ 0]^T$, and $\mathbf{Uf} = [f_\phi \ f_x \ d_f \ l^2\dot{\theta}_1 \ d_f \ l^2\dot{\theta}_2]^T$ [17,26] are the state vector, the control input vector, and the friction/disturbance vector, respectively. The definitions of $\mathbf{M}(\mathbf{q})$, $\mathbf{C}(\mathbf{q}, \dot{\mathbf{q}})$, and $\mathbf{G}(\mathbf{q})$ are provided in [2].

The dynamics of 4DOF tower cranes (see Fig. 1) can be further expressed as follows [21]:

$$\begin{aligned} & 2(M+m)x\dot{\phi}\dot{x} - ml\ddot{\phi}\dot{x}\theta_2 + 2ml\dot{\phi}\dot{x}\theta_1 + ml^2\dot{\phi}\theta_2^2 + mlx\ddot{\theta}_2 \\ & + (M+m)x^2\ddot{\phi} + 2mxl\ddot{\phi}\theta_1 + ml^2\dot{\phi}\theta_1^2 + 2mxl\dot{\phi}\theta_1 + ml^2\dot{\phi}_2\dot{\theta}_1 \\ & + 2ml^2\dot{\phi}\dot{\theta}_1\theta_1 - ml^2\dot{\theta}_1\theta_2 + ml^2\dot{\theta}_1^2\theta_1\theta_2 - 2mxl\dot{\phi}\dot{\theta}_2\theta_1\theta_2 - mlx\dot{\theta}_2^2\theta_2 \\ & - 2ml^2\dot{\phi}\dot{\theta}_2\theta_1^2\theta_2 + 2ml^2\dot{\phi}\dot{\theta}_2\theta_2 - ml^2\dot{\theta}_1\dot{\theta}_2 + ml^2\dot{\theta}_2\theta_1 + ml^2\dot{\theta}_1\dot{\theta}_2\theta_2^2 + J\ddot{\phi} = u_\phi - f_\phi \end{aligned} \quad (2)$$

$$\begin{aligned} & (M+m)\ddot{x} - (M+m)\dot{\phi}^2x - ml\dot{\phi}^2\theta_1 - m\ddot{\phi}l\theta_2 + m\ddot{\theta}_1l \\ & - m\ddot{\theta}_1^2l\theta_1 - 2m\dot{\theta}_1\dot{\theta}_2l\theta_2 - 2m\dot{\phi}\dot{\theta}_2l - m\ddot{\theta}_2l\theta_1\theta_2 - m\ddot{\theta}_2^2l\theta_1 = u_x - f_x \end{aligned} \quad (3)$$

$$ml\ddot{x} + ml^2\ddot{\theta}_1 - mxl\ddot{\phi} - m\dot{\phi}^2l^2\theta_1 - 2ml^2\dot{\phi}\dot{\theta}_2 - 2ml^2\dot{\theta}_2\dot{\theta}_1\dot{\theta}_2 - ml^2\theta_2\ddot{\phi} = -mgl\theta_1 - d_f l^2\dot{\theta}_1 \quad (4)$$

$$\begin{aligned} & ml^2\ddot{\theta}_2 - ml\theta_2\theta_1\ddot{x} + 2ml\dot{x}\dot{\phi} + xml\ddot{\phi} + 2ml^2\dot{\phi}\dot{\theta}_1 + ml^2\theta_1\ddot{\phi} \\ & + mxl\theta_2\theta_1\dot{\phi}^2 + ml^2\theta_2\dot{\theta}_1^2\dot{\phi}^2 - ml^2\theta_2\dot{\phi}^2 + ml^2\theta_2\dot{\theta}_1^2 = -mgl\theta_2 - d_f l^2\dot{\theta}_2 \end{aligned} \quad (5)$$

The expressions of the friction torque f_ϕ and friction force f_x are defined as follows [7,22,24,25]:

$$f_\phi = f_{0\phi}\tanh\left(\frac{\dot{\phi}}{\varepsilon_{0\phi}}\right) + k_{0\phi}|\dot{\phi}|\dot{\phi}, \quad (6)$$

$$f_x = f_{0x}\tanh\left(\frac{\dot{x}}{\varepsilon_{0x}}\right) + k_{0x}|\dot{x}|\dot{x}, \quad (7)$$

with $f_{0\phi}$, $\varepsilon_{0\phi}$, $k_{0\phi}$, f_{0x} , ε_{0x} , and k_{0x} being friction-related parameters.

The detailed state variables and parameters in the dynamic equation are illustrated in Table 1.

2.2. Auxiliary signals design

To facilitate the trajectory planning process, some new auxiliary terms are designed to express state variables of tower crane systems. According to the geometrical relationships in Fig. 1, the trolley positions in the coordinate frame are denoted by

$$x_M = x\cos\phi \quad (8)$$

$$y_M = x\sin\phi \quad (9)$$

Furthermore, the payload coordinates can be calculated as

$$x_m = x\cos\phi + l\cos\theta_2\sin\theta_1\cos\phi - l\sin\theta_2\sin\phi \quad (10)$$

$$y_m = x\sin\phi + l\cos\theta_2\sin\theta_1\sin\phi + l\sin\theta_2\cos\phi \quad (11)$$

Taking into account the constraint on the swing angle within a small range, Eqs.(10) and (11) can be further rewritten (when the swing angle is sufficiently small, Eqs.(10) and (11) can use the following approximations: $\sin\theta_1 \simeq \theta_1$, $\sin\theta_2 \simeq \theta_2$, $\cos\theta_1 \simeq 1$, $\cos\theta_2 \simeq 1$):

Table 1

Parameters and variables.

| Symbols | Physical meaning | Units |
|----------------------|---|----------------|
| x, x_r | trolley displacement and trolley reference trajectory | m |
| ϕ, ϕ_r | jib slew angle and jib reference trajectory | rad |
| x_0, x_d | the initial and desired positions of the trolley | m |
| ϕ_0, ϕ_d | the initial and desired positions of the jib | rad |
| x_1, y_1 | the x-axis and y-axis positions of the obstacle | m |
| θ_1, θ_2 | payload swing angles | rad |
| l | cable length | m |
| M, m | trolley and payload masses | kg |
| g | gravity constant | m/s^2 |
| J | jib moment inertia | $kg \cdot m^2$ |
| u_ϕ | torque controlling jib slew | $N \cdot m$ |
| u_x | force controlling trolley translation displacement | N |
| d_f | air resistance coefficient | -- |

$$x_m = x \cos \phi + l \theta_1 \cos \phi - l \theta_2 \sin \phi \quad (12)$$

$$y_m = x \sin \phi + l \theta_1 \sin \phi + l \theta_2 \cos \phi \quad (13)$$

The second time derivative of Eqs.(12) and (13) can be expressed as:

$$\begin{aligned} \ddot{x}_m &= \ddot{x} \cos \phi - 2 \dot{x} \dot{\phi} \sin \phi - x \dot{\phi}^2 \cos \phi - x \ddot{\phi} \sin \phi + l \ddot{\theta}_1 \cos \phi \\ &\quad - l \ddot{\theta}_2 \sin \phi - 2 l \dot{\theta}_1 \dot{\phi} \sin \phi - 2 l \dot{\theta}_2 \sin \phi - 2 l \dot{\theta}_2 \dot{\phi} \cos \phi \\ &\quad - l \theta_1 \ddot{\phi} \sin \phi - l \theta_1 \dot{\phi}^2 \cos \phi - l \theta_2 \ddot{\phi} \cos \phi + l \theta_2 \dot{\phi}^2 \sin \phi \end{aligned} \quad (14)$$

$$\begin{aligned} \ddot{y}_m &= \ddot{x} \sin \phi + 2 \dot{x} \dot{\phi} \cos \phi - x \dot{\phi}^2 \sin \phi + x \ddot{\phi} \cos \phi + l \ddot{\theta}_1 \sin \phi \\ &\quad + l \ddot{\theta}_2 \cos \phi + 2 l \dot{\theta}_1 \dot{\phi} \cos \phi - 2 l \dot{\theta}_2 \dot{\phi} \sin \phi + l \theta_1 \dot{\phi} \cos \phi \\ &\quad - l \theta_1 \dot{\phi}^2 \sin \phi - l \theta_2 \ddot{\phi} \sin \phi - l \theta_2 \dot{\phi}^2 \cos \phi \end{aligned} \quad (15)$$

Eqs.(14) and (15) are further processed and

$$\ddot{x}_m \cos \phi + \ddot{y}_m \sin \phi = \ddot{x} - x \dot{\phi}^2 + l \ddot{\theta}_1 + 2 l \dot{\theta}_1 - 2 l \dot{\theta}_2 \dot{\phi} - l \theta_1 \dot{\phi}^2 - l \theta_2 \dot{\phi} \quad (16)$$

$$\ddot{x}_m \sin \phi - \ddot{y}_m \cos \phi = -2 \dot{x} \dot{\phi} - x \ddot{\phi} - l \ddot{\theta}_2 - 2 l \dot{\theta}_1 \dot{\phi} - l \theta_1 \ddot{\phi} + l \theta_2 \dot{\phi}^2. \quad (17)$$

According to Eqs.(4), (5), (16), and (17), the following relationships can be obtained

$$\ddot{x}_m \cos \phi + \ddot{y}_m \sin \phi = -g \theta_1 \quad (18)$$

$$\ddot{x}_m \sin \phi - \ddot{y}_m \cos \phi = g \theta_2 \quad (19)$$

On the other hand, from Eqs.(12) and (13), the variables θ_1 and θ_2 can be calculated as follows:

$$\theta_1 = \frac{1}{l} (x_m \cos \phi + y_m \sin \phi - x) \quad (20)$$

$$\theta_2 = \frac{1}{l} (y_m \cos \phi - x_m \sin \phi) \quad (21)$$

Then, after multiplying Eqs.(18) and (19) by $\cos \phi$ and $\sin \phi$ respectively, and combining with Eqs. (9), (20), and (21), the expression of ϕ can be derived below

$$\begin{aligned} \ddot{x}_m \cos \phi^2 + \ddot{x}_m \sin \phi^2 &= g(-\theta_1 \cos \phi + \theta_2 \sin \phi) \\ \Rightarrow \ddot{x}_m &= -\frac{g}{l} x_m + \frac{g}{l} x \cos \phi \\ \Rightarrow \left(\ddot{x}_m + \frac{g}{l} x_m \right) \tan(\phi) &= \frac{g}{l} y_M \\ \Rightarrow \phi &= \arctan \varphi \end{aligned} \quad (22)$$

where $\varphi = y_M / \left(\frac{l}{g} \ddot{x}_m + x_m \right)$.

Substituting Eq.(22) into the expression for y_M in Eq.(9) results in,

$$x = \frac{y_M}{\sin(\arctan \varphi)} \quad (23)$$

Subsequently, Eq.(22) is substituted into Eqs.(20) and (21) to derive that

$$\theta_1 = \frac{1}{l} [x_m \cos(\arctan \varphi) + y_m \sin(\arctan \varphi) - x] \quad (24)$$

$$\theta_2 = \frac{1}{l} [y_m \cos(\arctan \varphi) - y_m \sin(\arctan \varphi)] \quad (25)$$

The results above Eqs.(22)-(25) indicate that all state variables of the tower crane system can be represented by x_m , y_m , and y_M . These auxiliary terms are utilized to express the functions of state variable constraints and reference trajectory, which are crucial in solving the optimization problem.

3. Trajectory planning

In this part, constraint equations are formulated, and the trajectory parameters can be obtained by solving these equations. Subsequently, an optimization problem is established, expressed using auxiliary terms. And then, the FNN-based trajectory is derived

based on the optimization problem. Fig. 2 give the process of obstacle avoidance, and from which, it clearly observed that the collisions can be avoided by tracking the FNN-based trajectory.

3.1. Optimization problem construction

To realize precise positioning and swing elimination, the constraint equations of physical signals are set as follows:

$$x_m(0) = x_{m0}x_m^{(i)}(0) = 0x_m(t_f) = x_{md}x_m^{(i)}(t_f) = 0 \quad (26)$$

$$y_m(0) = y_{m0}y_m^{(i)}(0) = 0y_m(t_f) = y_{md}y_m^{(i)}(t_f) = 0 \quad (27)$$

$$y_M(0) = y_{M0}, y_M^{(j)}(0) = 0, y_M(t_f) = y_{Md}y_M^{(j)}(t_f) = 0 \quad (28)$$

where $i = 1, 2, 3, 4, 5$, and $j = 1, 2, 3$, and the start positions of the payload x_{m0} (x-axis position) and y_{m0} (y-axis position); the target positions x_{md} and y_{md} ; the initial and final positions of the trolley y_{M0} and y_{Md} , respectively. In detail, $x_{m0} = x_0\cos\phi_0$, $x_{md} = x_d\cos\phi_d$, $y_{m0} = x_0\sin\phi_0$, $y_{md} = x_d\sin\phi_d$, $y_{M0} = x_0\sin\phi_0$, and $y_{Md} = x_d\sin\phi_d$, respectively.

To ensure safety and trackability, the state variables should be restricted in appropriate ranges, i.e.,

$$|\dot{\phi}(t)| \leq v_{\phi\max}, |\ddot{\phi}(t)| \leq a_{\phi\max} \quad (29)$$

$$|\dot{x}(t)| \leq v_{x\max}, |\ddot{x}(t)| \leq a_{x\max} \quad (29)$$

$$|\theta_1(t)| \leq k_{\theta1\max}, |\theta_2(t)| \leq k_{\theta2\max} \quad (29)$$

where $v_{\phi\max}$, $a_{\phi\max}$, $v_{x\max}$, $a_{x\max}$, $k_{\theta1\max}$ and $k_{\theta2\max}$ are the physical signal constraint boundaries of the jib angle, the trolley displacement, and the swing angles, respectively.

To satisfy Eq. (29), an optimal trajectory further is designed with minimum transportation time. Next, the auxiliary signals x_m , y_m , and y_M , will be parameterized by appropriate functions. To ensure trajectory accuracy, the reference trajectories x_m and y_m are selected as eleven-order polynomial curves, and a seven-order polynomial curve is chosen as the y-axis of the desired trolley trajectory, with the following expression:

$$\begin{cases} x_m(t) = x_{m0} + (x_{md} - x_{m0}) \sum_{i=0}^{11} \alpha_i t^i \\ y_m(t) = y_{m0} + (y_{md} - y_{m0}) \sum_{i=0}^{11} \beta_i t^i \\ y_M(t) = y_{M0} + (y_{Md} - y_{M0}) \sum_{j=0}^7 \eta_j t^j \end{cases} \quad (30)$$

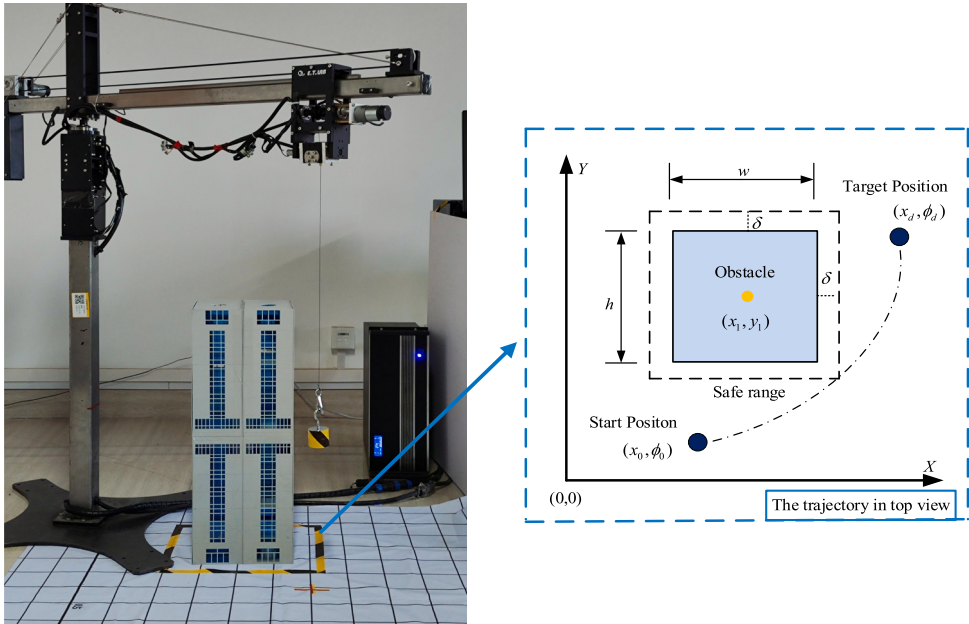


Fig. 2. The designed obstacle avoidance trajectory in front and top view.

where $\alpha_i, \beta_i, i=\{1, \dots, 11\}$ and $\eta_j, j=\{1, \dots, 9\}$, are to-be-determined parameters. And $\tau = \frac{t}{t_f}$ represents the time-dependent normalization parameter, wherein t_f denotes the optimal transportation time.

The nth-order derivative of Eq. (30) gives the following results:

$$\begin{cases} x_m^{(p)}(t) = (x_{md} - x_{m0}) \sum_{i=6}^{11} \alpha_i \frac{i! \tau^{i-p}}{(i-p)! t_f^p} \\ y_m^{(p)}(t) = (y_{md} - y_{m0}) \sum_{i=6}^{11} \beta_i \frac{i! \tau^{i-p}}{(i-p)! t_f^p} \\ y_M^{(q)}(t) = (y_{Md} - y_{M0}) \sum_{j=4}^7 \eta_j \frac{j! \tau^{j-q}}{(j-p)! t_f^q} \end{cases} \quad (31)$$

wherein $p = 1, 2, 3, 4, 5$, and $q = 1, 2, 3$.

Substituting Eqs.(26)-(28) into Eqs.(30) and (31), the parameters can be obtained

$$\alpha_1 = \alpha_2 = \alpha_3 = \alpha_4 = \alpha_5 = 0, \beta_1 = \beta_2 = \beta_3 = \beta_4 = \beta_5 = 0, \eta_1 = \eta_2 = \eta_3 = 0$$

$$\alpha_6 = \beta_6 = 462\alpha_7 = \beta_7 = -1980\alpha_8 = \beta_8 = 3465\alpha_9 = \beta_9 = -3080$$

$$\alpha_{10} = \beta_{10} = 1386\alpha_{11} = \beta_{11} = -252\eta_4 = 35\eta_5 = -84\eta_6 = 70\eta_7 = -20 \quad (32)$$

Consequently, the expanded expression of all constraints in Eq.(29) can be derived from Eqs.(22)-(25) and (30)-(32). After substituting Eqs.(30)-(32) into Eqs.(22)-(25), the constraint functions are expressed by auxiliary terms x_m , y_m , and y_M . A series of constraint problems are translated into solving the minimum value of t_f . t_1 and t_2 represent the upper and lower limits of t_f , respectively, and ϵ denotes the maximum error. Then, the minimum time can be found to solve Eq.(33) utilizing a bisection-based method:

minimum t_f , subject to Eq. (29) (33)

Next, the obstacle is supposed to appear on the movement path at the moment t_s . To avoid collisions, the payload position should reach the right bottom of the safe range at the moment t_s . So, the obstacle avoidance trajectories of x_m , y_m , and y_M are designed as

$$x_m(t) = \begin{cases} x_{m0} + (x_{m1} - x_{m0}) \sum_{i=0}^{11} \alpha_i \left(\frac{t}{t_s}\right)^i, & 0 \leq t < t_s \\ x_{m1} + (x_{md} - x_{m1}) \sum_{i=0}^{11} \alpha_i \left(\frac{t - t_s}{t_f - t_s}\right)^i, & t_s \leq t \leq t_f \end{cases} \quad (34)$$

$$y_m(t) = \begin{cases} y_{m0} + (y_{m1} - y_{m0}) \sum_{i=0}^{11} \beta_i \left(\frac{t}{t_s}\right)^i, & 0 \leq t < t_s \\ y_{m1} + (y_{md} - y_{m1}) \sum_{i=0}^{11} \beta_i \left(\frac{t - t_s}{t_f - t_s}\right)^i, & t_s \leq t \leq t_f \end{cases} \quad (35)$$

$$y_M(t) = y_{M0} + (y_{Md} - y_{M0}) \sum_{j=0}^7 \eta_j \tau^j, \quad 0 \leq t < t_f \quad (36)$$

wherein $x_{m1} = x_1 + (\frac{w}{2} + \delta)$ and $y_{m1} = y_1 - (\frac{h}{2} + \delta)$, with w and h being the length and width of the obstacle, respectively. Moreover, t_s is the solution of the following equation:

$$x(t_s) = \sqrt{x_{m1}^2 + y_{m1}^2}. \quad (37)$$

By substituting Eqs. (34)–(36) into Eqs. (22) and (23), the final trajectories of $\phi_r(t)$ and $x_r(t)$ can be obtained.

3.2. Fnn-based obstacle avoidance trajectory design

FNN combines the advantages of fuzzy logic control reasoning and neural network fault tolerance. It employs the nonlinear mapping of the neural network, and self-learning ability to adapt fuzzy logic. FNN adjusts the weights and membership functions of the fuzzy system using an optimization algorithm.

The traditional trajectory planning method needs to calculate the time previously, which is tedious and time-consuming. In this part, FNN is incorporated in designing the obstacle avoidance trajectory instead of the traditional planning method. FNN could gain the optimal time directly once the fuzzy logic input variables are established. Furthermore, it eliminates the complex calculations typically required by traditional methods, thereby simplifying the trajectory planning process. In conclusion, FNN significantly enhances the

efficiency of trajectory planning by reducing computation compared to traditional approaches.

The time parameters and reference trajectory can be predicted through trained FNN, necessitating only the position parameters without calculations. As depicted in [Appendix A](#), forty groups of collected data are utilized to train FNN. The t_f and t_s data sets are calculated and collected in [Section 3.1](#). By utilizing the training data, FNN constructs a nonlinear mapping between input variables x_d , ϕ_d , x_1 , and y_1 and output variables t_f and t_s . The structure of the used FNN, as depicted in [Fig. 3](#), consists of five layers. Additionally, eight groups of testing data will be generated randomly within the input ranges described in [Fig. 3](#). The testing data is utilized to test the prediction performance of FNN. The composition and function of each layer are described below.

Layer 1: Input layer. In this layer, there are 4 nodes: the target positions of payload x_d and ϕ_d , the obstacle center positions x_1 and y_1 . The input ranges of 4 nodes are $x_d \in [0.5, 0.68]$, $\phi_d \in [45, 55]$, $x_1 \in [0.07, 0.25]$, and $y_1 \in [0.2, 0.38]$, respectively.

Layer 2: The fuzzifier layer. The Gaussian functions are used as fuzzy functions. Every input variable has 4 fuzzy sets, i.e., PL (positive large), PS (positive small), NS (negative small), and NL (negative large). This layer comprises 16 nodes.

$$u_{ij} = e^{-((x(i)-a_{ij})/b_{ij})^2} \quad (38)$$

where u_{ij} and $x(i)$ denote note output data and input data, a_{ij} and b_{ij} respectively represent the centroid and width of affiliation functions, $i=j = 1, 2, 3, 4$.

Layer 3: The inference layer. This layer consists of 256 nodes, each representing a fuzzy rule.

$$\alpha_m(t) = \prod_{i=1}^{i=j=4} \mu_{ij}(t) \quad (39)$$

where $\alpha_m(t)$ denotes the output of the third layer.

Layer 4: The normalization layer. Subsequently, the notes of the rule generation layer are normalized in this layer. The number of notes in this layer is similar to the layer 4.

$$\beta_m = \frac{\alpha_m}{\sum_{m=1}^{256} \alpha_m} \quad (40)$$

Layer 5: The output layer. A weighted average method is used to defuzzify β_m .

| ϕ_d | x_d | x_1 | y_1 | t_f | t_s |
|----------|-------|-------|-------|--------|--------|
| 0.5 | 45 | 0.2 | 0.32 | 6.5134 | 3.6584 |
| 0.52 | 45 | 0.2 | 0.32 | 6.6763 | 3.6357 |
| 0.54 | 45 | 0.2 | 0.32 | 6.8320 | 3.6180 |
| 0.56 | 45 | 0.2 | 0.32 | 6.9785 | 3.6026 |
| 0.58 | 45 | 0.2 | 0.32 | 7.1194 | 3.5903 |
| ... | ... | ... | ... | ... | ... |
| 0.65 | 47 | 0.16 | 0.32 | 7.5607 | 3.2839 |
| 0.65 | 47 | 0.16 | 0.34 | 7.5607 | 3.3513 |
| 0.65 | 47 | 0.16 | 0.36 | 7.5607 | 3.4244 |
| 0.65 | 47 | 0.16 | 0.38 | 7.5607 | 3.5027 |

Training data

```

 $a_g = [[1.19717354, 1.36446151, ..., -0.4221005, -1.07603388]]$ 
 $b_g = [[0.90956569, -0.285172, ..., 0.06797926, -1.54968994]]$ 
 $w_m = [1.69334934e+00, ..., 7.31466846e-01, 8.05097857e-01]$ 
 $a_o = [[-1.8963831, -0.39244347, ..., -1.52204845, -0.9844266]]$ 
 $b_o = [[-1.83918734, -1.2294696, ..., 1.64330207, -0.88809536]]$ 
 $w_m = [1.69334934e+00, ..., 7.31466846e-01, 8.05097857e-01]$ 

```

FNN coefficients

| ϕ_d | x_d | x_1 | y_1 | t_f | t_s |
|----------|-------|-------|-------|--------|--------|
| 0.51 | 45 | 0.2 | 0.32 | 6.5958 | 3.6462 |
| 0.54 | 47 | 0.19 | 0.31 | 6.8246 | 3.5036 |
| 0.6 | 51 | 0.22 | 0.32 | 7.2293 | 3.7100 |
| 0.62 | 50 | 0.2 | 0.35 | 7.3630 | 3.6539 |
| 0.6 | 55 | 0.18 | 0.34 | 7.2110 | 3.4823 |
| 0.65 | 52 | 0.21 | 0.33 | 7.5351 | 3.6379 |
| 0.6 | 49 | 0.16 | 0.34 | 7.2385 | 3.3576 |
| 0.66 | 46 | 0.2 | 0.36 | 7.6248 | 3.6763 |

Testing data

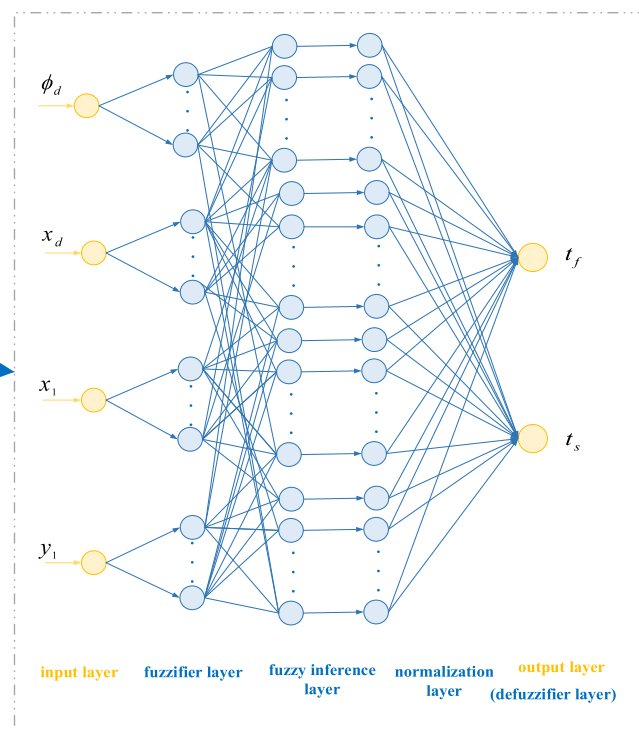


Fig. 3. The structure of the FNN (The entire training data is displayed in [Appendix A](#)).

$$y = \sum_{m=1}^{256} \beta_m w_m \quad (41)$$

in which, w_m denotes the connection weight coefficients between the fourth and fifth layers.

Following optimization, the centroid and width of membership functions a_{ij} and b_{ij} , along with the connection weight coefficients w_m , are updated iteratively. The detailed coefficients a_{ij} , b_{ij} , and w_m are given in [Appendix B](#). The prediction performance of FNN is evaluated by using four model evaluation indexes, namely, MAE, RMSE, MAPE, and SMAPE, which are described in [Table 2](#). In addition, the prediction result of testing data is illustrated in [Table 3](#).

4. Controller design

In this section, to follow the desired trajectory precisely, an adaptive tracking controller is designed for 4DOF tower cranes with error constraints (the flowchart is shown in [Fig. 4](#)).

For system (1), an appropriate controller is designed to achieve the following goals:

- The jib and the trolley can achieve accurate positioning, and the payload swing can be suppressed to zero, i.e.,

$$\lim_{t \rightarrow t_f} [\phi \quad x \quad \dot{\phi} \quad \dot{x}]^T = [\phi_r \quad x_r \quad 0 \quad 0]^T \quad (42)$$

$$\lim_{t \rightarrow \infty} [\theta_1 \quad \theta_2 \quad \dot{\theta}_1 \quad \dot{\theta}_2]^T = [0 \quad 0 \quad 0 \quad 0]^T \quad (43)$$

wherein t_f represents the expected transportation time, which can be calculated by Algorithm 1. And ϕ_r and x_r are the reference trajectories based on Eqs.(22), (23), and (34)-(36).

- Throughout the control process, the tracking errors of the jib and the trolley are limited to small ranges:

$$-a < e_\phi < a - b < e_x < b \quad (44)$$

wherein e_ϕ and e_x represent the jib and the trolley tracking errors, respectively:

$$e_\phi = \phi - \phi_r \quad (45)$$

$$e_x = x - x_r \quad (46)$$

with a and b standing for the bounds of e_ϕ and e_x , respectively.

To guarantee the tracking performance, the following conditions should be satisfied. The reference trajectories of the jib and the trolley should vary from their initial positions at $t = 0$ to their target positions at $t = t_f$. Additionally, all speed and acceleration signals of the jib and the trolley should also be zero at the time $t = 0$ and $t = t_f$. Consequently, the following conditions are imposed:

$$\begin{aligned} \phi_r(t)\dot{\phi}_r(t)\ddot{\phi}_r(t)x_r(t)\dot{x}_r(t)\ddot{x}_r(t) &\in L_\infty \\ \phi_r(0) = \phi_0\phi_r^{(k)}(0) = 0, \phi_r(t) = \phi_d\phi_r^{(k)}(t) = 0 \\ x_r(0) = x_0, x_r^{(k)}(0) = 0, x_r(t) = x_d, x_r^{(k)}(t) = 0, k = 1, 2, 3, \text{when } t \geq t_f \end{aligned} \quad (47)$$

4.1. Trajectory-tracking controller design

Similar to the structure of the system energy function, the error-based scalar function is defined as follows:

$$V_E = \frac{1}{2}\dot{\mathbf{q}}_e^T \mathbf{M}(\mathbf{q})\dot{\mathbf{q}}_e + mgl(1 - \cos\theta_1 \cos\theta_2) \quad (48)$$

wherein $\mathbf{q}_e = [e_\phi \quad e_x \quad \theta_1 \quad \theta_2]^T$ refers to the error vector.

The time derivative of V_E can be written as

Table 2

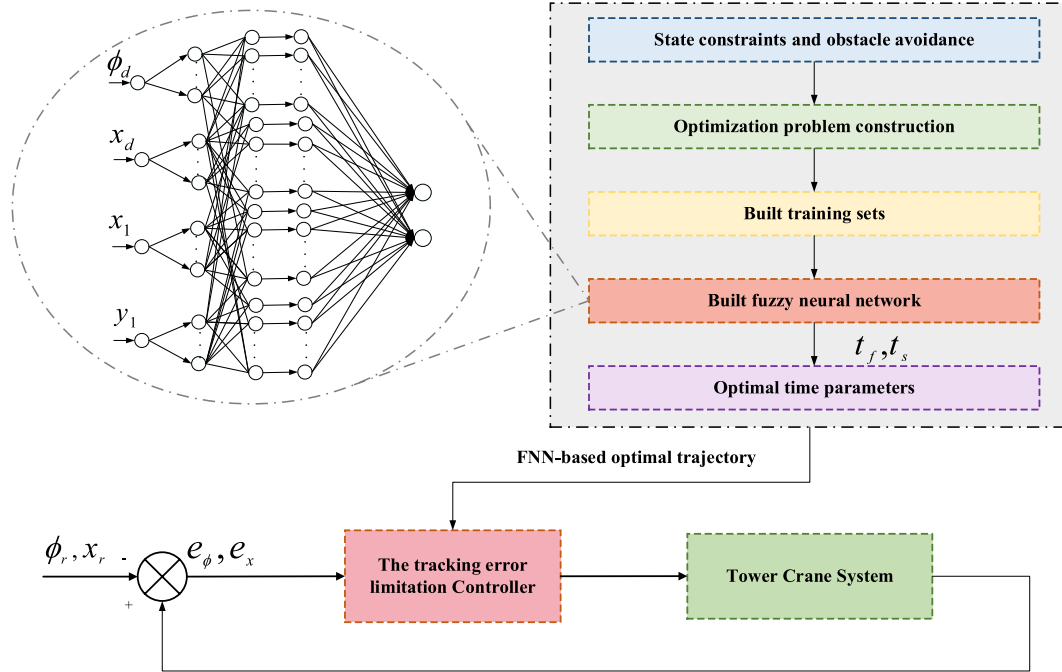
Model evaluation indexes.

| Parameters | MAE | RMSE | MAPE | SMAPE |
|------------|---------|---------|--------|--------|
| t_f | 0.01904 | 0.02602 | 0.26 % | 0.26 % |
| t_s | 0.04760 | 0.07148 | 1.35 % | 1.33 % |

Table 3

The results of FNN prediction.

| Parameters | 1 | 2 | 3 | 4 | 5 | 6 | 7 | 8 |
|------------|------|------|------|------|------|------|------|------|
| t_f | 6.60 | 6.84 | 7.22 | 7.36 | 7.27 | 7.50 | 7.25 | 7.61 |
| t_s | 3.64 | 3.53 | 3.65 | 3.65 | 3.66 | 3.63 | 3.41 | 3.63 |

**Fig. 4.** The block diagram of the designed control system.

$$\begin{aligned}
\dot{V}_E &= \ddot{\mathbf{q}}_e^T \mathbf{M}(\mathbf{q}) \ddot{\mathbf{q}}_e + \frac{1}{2} \dot{\mathbf{q}}_e^T \dot{\mathbf{M}}(\mathbf{q}) \dot{\mathbf{q}}_e + mg l \sin \theta_1 \cos \theta_2 \dot{\theta}_1 + mg l \cos \theta_1 \sin \theta_2 \dot{\theta}_2 \\
&= \ddot{\mathbf{q}}_e^T \mathbf{M}(\mathbf{q}) \ddot{\mathbf{q}}_e + \ddot{\mathbf{q}}_e^T \mathbf{C}(\mathbf{q}, \dot{\mathbf{q}}) \dot{\mathbf{q}}_e + mg l \sin \theta_1 \cos \theta_2 \dot{\theta}_1 + mg l \cos \theta_1 \sin \theta_2 \dot{\theta}_2 \\
&= \ddot{\mathbf{q}}_e^T (\mathbf{M}(\mathbf{q}) \ddot{\mathbf{q}}_e + \mathbf{C}(\mathbf{q}, \dot{\mathbf{q}}) \dot{\mathbf{q}}_e) + mg l \sin \theta_1 \cos \theta_2 \dot{\theta}_1 + mg l \cos \theta_1 \sin \theta_2 \dot{\theta}_2 \\
&= \ddot{\mathbf{q}}_e^T (\mathbf{M}(\mathbf{q}) \ddot{\mathbf{q}} + \mathbf{C}(\mathbf{q}, \dot{\mathbf{q}}) \dot{\mathbf{q}} - \mathbf{M}(\mathbf{q}) \ddot{\mathbf{q}}_r - \mathbf{C}(\mathbf{q}, \dot{\mathbf{q}}) \dot{\mathbf{q}}_r) + mg l \sin \theta_1 \cos \theta_2 \dot{\theta}_1 + mg l \cos \theta_1 \sin \theta_2 \dot{\theta}_2 \\
&= -\ddot{\mathbf{q}}_e^T (\mathbf{U} - \mathbf{U}_f - \mathbf{G}(\mathbf{q}) - \mathbf{M}(\mathbf{q}) \ddot{\mathbf{q}}_r - \mathbf{C}(\mathbf{q}, \dot{\mathbf{q}}) \dot{\mathbf{q}}_r) + mg l \sin \theta_1 \cos \theta_2 \dot{\theta}_1 + mg l \cos \theta_1 \sin \theta_2 \dot{\theta}_2
\end{aligned} \tag{49}$$

After simplifying a little, Eq.(49) can be expressed as follows:

$$\dot{V}_E = -\ddot{\mathbf{q}}_e^T (\mathbf{U} - \mathbf{U}_f - \mathbf{M}(\mathbf{q}) \ddot{\mathbf{q}}_r - \mathbf{C}(\mathbf{q}, \dot{\mathbf{q}}) \dot{\mathbf{q}}_r) \tag{50}$$

where $\mathbf{q}_r = [\phi_r \ x_r \ 0 \ 0]^T$ is the reference vector of \mathbf{q} .

By substituting the Eq.(1) into Eq.(50) and after tedious simplification, one has

$$\dot{V}_E = \left(u_\phi - \omega_\phi^T \mathbf{Z}(\phi) \right) \dot{e}_\phi + \left(u_x - \omega_x^T \mathbf{Z}(x) \right) \dot{e}_x + A + B \tag{51}$$

with $\omega_\phi^T = [f_{0\phi} \ k_{0\phi} \ ml^2 \ ml \ m+M \ J]$, $\mathbf{Z}(\phi)^T = \left[\tanh\left(\frac{\dot{\phi}}{\varepsilon_{0\phi}}\right) \ |\dot{\phi}| \dot{\phi} \ Z_{\phi 1} \ Z_{\phi 2} \ Z_{\phi 3} \ \ddot{\phi}_r \right]$, $\omega_x^T = [f_{0x} \ k_{0x} \ ml \ m+M]$, and $\mathbf{Z}(x)^T = \left[\tanh\left(\frac{\dot{x}}{\varepsilon_{0x}}\right) \ |\dot{x}| \dot{x} \ -\theta_2 \ddot{\phi}_r - \theta_1 \dot{\phi} \dot{\phi}_r - \dot{\theta}_2 \dot{\phi}_r \ \ddot{x}_d - x \dot{\phi} \dot{\phi}_r \right]$.

And $Z_{\phi 1} = (\theta_1^2 + \theta_2^2) \dot{\phi}_r + \theta_1 \dot{\theta}_1 \dot{\phi}_r + \theta_2 \dot{\theta}_2 \dot{\phi}_r$, $Z_{\phi 2} = 2x \theta_1 \theta_2 \ddot{\phi}_r - \theta_2 \ddot{x}_r + x \dot{\theta}_1 \dot{\phi}_r + \theta_1 \dot{x}_r \dot{\phi}_r + \theta_1 \dot{\phi} \dot{\phi}_r + \dot{\theta}_2$ and $Z_{\phi 3} = x^2 \ddot{\phi}_r + x \dot{x} \dot{\phi}_r + x \dot{\phi} \dot{\phi}_r$.The expressions of A and B are as follows:

$$\begin{aligned} A &= -d_f l^2 \dot{\theta}_1^2 + ml^2 \theta_2 \ddot{\phi}_r \dot{\theta}_1 - ml \ddot{x}_r \dot{\theta}_1 - d_f \dot{x}_r l \dot{\theta}_1 \\ &\quad + ml(x + l\theta_1) \dot{\phi}_r \dot{\theta}_1 + ml^2 \dot{\phi}_r \dot{\theta}_1 \dot{\theta}_2 \\ B &= -d_f l^2 \dot{\theta}_2^2 + d_f \dot{x}_r l \theta_1 \theta_2 \dot{\theta}_2 - ml(x + l\theta_1) \ddot{\phi}_r \dot{\theta}_2 + ml\theta_1 \theta_2 \ddot{x}_r \dot{\theta}_2 - 2ml \dot{\phi}_r \dot{x}_r \dot{\theta}_2 - ml(x\theta_1 \theta_2 - l\theta_2) \dot{\phi}_r^2 \dot{\theta}_2 - ml\dot{\theta}_1 \dot{\phi}_r \dot{\theta}_2 \end{aligned} \quad (52)$$

Our control laws can be formulated as follows:

$$\begin{aligned} u_\phi &= -k_{p\phi} e_\phi - k_{d\phi} \dot{e}_\phi - \widehat{\omega}_\phi^T Z(\phi) - \lambda_1 \frac{e_\phi}{a^2 - e_\phi^2} \\ u_x &= -k_{px} e_x - k_{dx} \dot{e}_x - \widehat{\omega}_x^T Z(x) - \lambda_2 \frac{e_x}{b^2 - e_x^2} \end{aligned} \quad (53)$$

wherein $k_{p\phi}$, $k_{d\phi}$, k_{px} , and $k_{dx} \in R^+$ represent positive control gains; λ_1 and $\lambda_2 \in R^+$ are the positive parameters; $\widehat{\omega}_\phi \in R^{6 \times 1}$ and $\widehat{\omega}_x \in R^{4 \times 1}$ respectively denote the estimations for uncertain parameter vectors ω_ϕ and ω_x , with the following explicit expressions:

$$\begin{aligned} \widehat{\omega}_\phi^T &= [\widehat{f}_{0\phi} \quad \widehat{k}_{0\phi} \quad \widehat{ml}^2 \quad \widehat{ml} \quad \widehat{m+M} \quad \widehat{J}] \\ \widehat{\omega}_x^T &= [\widehat{f}_{0x} \quad \widehat{k}_{0x} \quad \widehat{ml} \quad \widehat{m+M}] \end{aligned}$$

The adaptive laws of $\widehat{\omega}_\phi$ and $\widehat{\omega}_x$ are as follows:

$$\begin{aligned} \dot{\widehat{\omega}}_x &= \Lambda_1 Z(\phi) \dot{e}_\phi \\ \dot{\widehat{\omega}}_\phi &= \Lambda_2 Z(x) \dot{e}_x \end{aligned} \quad (54)$$

where $\Lambda_1 \in R^{6 \times 6}$ and $\Lambda_2 \in R^{4 \times 4}$ denote non-negative definite diagonal matrixes.

4.2. Stability analysis

Theorem 1. The proposed controller can satisfy the following control objective.

$$\lim_{t \rightarrow \infty} [e_\phi \quad e_x \quad \theta_1 \quad \theta_2]^T = [0 \quad 0 \quad 0 \quad 0]^T \quad (55)$$

Proof. To prove the stability of tower crane systems, the non-negative scalar function is defined as follows:

$$V_{all} = V_E + \frac{1}{2} k_{p\phi} e_\phi^2 + \frac{1}{2} k_{px} e_x^2 + \frac{1}{2} \widetilde{\omega}_\phi^T \Lambda_\phi^{-1} \widetilde{\omega}_\phi + \frac{1}{2} \widetilde{\omega}_x^T \Lambda_x^{-1} \widetilde{\omega}_x + \frac{1}{2} \lambda_1 \ln \frac{a^2}{a^2 - e_\phi^2} + \frac{1}{2} \lambda_2 \ln \frac{b^2}{b^2 - e_x^2} \quad (56)$$

The estimation errors $\widetilde{\omega}_\phi$ and $\widetilde{\omega}_x$ are defined as

$$\begin{aligned} \widetilde{\omega}_\phi &= \omega_\phi - \widehat{\omega}_\phi \\ \widetilde{\omega}_x &= \omega_x - \widehat{\omega}_x \end{aligned} \quad (57)$$

Taking the time derivative of Eq.(56), one has

$$\dot{V}_{all} = \dot{V}_E + k_{p\phi} e_\phi \dot{e}_\phi + k_{px} e_x \dot{e}_x - \widetilde{\omega}_\phi^T \Lambda_\phi \dot{\widetilde{\omega}}_\phi - \widetilde{\omega}_x^T \Lambda_x \dot{\widetilde{\omega}}_x \quad (58)$$

After substituting Eq.(49) into Eq.(58), it is obtained that

$$\dot{V}_{all} = -k_{d\phi} \dot{e}_\phi^2 - k_{dx} \dot{e}_x^2 + A + B. \quad (59)$$

$$A = -d_f l \dot{\theta}_1^2 B = -d_f l^2 \dot{\theta}_2^2 \text{ when } t \geq t_f \quad (60)$$

based on which, when $t > t_f$, Eq.(59) becomes

$$\dot{V}_{all} = -k_{d\phi} \dot{e}_\phi^2 - k_{dx} \dot{e}_x^2 - d_f l \dot{\theta}_1^2 - d_f l^2 \dot{\theta}_2^2 \leq 0, \quad (61)$$

Hence, Eq.(61) can derive

$$0 \leq V_{all}(0) \leq +\infty \Rightarrow V_{all}(t) \leq V_{all}(0) \leq +\infty. \quad (62)$$

Then, the following results can be concluded that

$$V_{all}(t) \in L_\infty \Rightarrow e_\phi, e_x, \dot{e}_\phi, \dot{e}_x, \dot{\theta}_1, \dot{\theta}_2, \widetilde{\omega}_\phi, \widetilde{\omega}_x, \ln \frac{a^2}{a^2 - e_\phi^2}, \ln \frac{b^2}{b^2 - e_x^2} \in L_\infty \quad (63)$$

Utilizing Eq.(47), together with $\omega_\phi, \omega_x \in L_\infty$, one can further obtain that

$$\hat{\omega}_\phi, \hat{\omega}_x, \phi, x, \dot{\phi}, \dot{x} \in L_\infty \Rightarrow Z(\phi), Z(x) \in L_\infty \quad (64)$$

Then, based on Eqs.(53), and (2)-(7), the following result can be obtained:

$$u_\phi, u_x, f_\phi, f_x \in L_\infty \Rightarrow \ddot{\phi}, \ddot{x}, \ddot{\theta}_1, \ddot{\theta}_2 \in L_\infty \quad (65)$$

According to Eq.(47), $e_\phi(0) = 0 < a$. Then, the trolley tracking error $|e_\phi|$ is supposed to tend to the boundedness a . Then one has $e_\phi(t) \rightarrow a^-$, and $V_{all}(t) \rightarrow +\infty$. The contractiveness can be demonstrated using equation Eqs.(56) and (62). Hence, as long as $e_\phi(0) = 0 < a$, one has

$$|e_\phi(t)| \rightarrow a^-, \quad \forall t \geq 0 \quad (66)$$

The corresponding analysis is conducted for e_x , i.e.,

$$|e_x(t)| \rightarrow b^-, \quad \forall t \geq 0 \quad (67)$$

Subsequently, LaSalle's invariance principle will be applied to conclude the stability analysis. To further establish asymptotic stability, an invariant set will be introduced in the following manner:

$$S \triangleq \left\{ (\mathbf{q}, \dot{\mathbf{q}}) | \dot{V}_{all} = 0 \right\} \quad (68)$$

and then, define the largest invariance set in S as Ω . Combining Eq.(61), the following result can be discovered:

$$\begin{aligned} \dot{\phi} &= 0, \quad \dot{e}_x = 0, \quad \dot{\theta}_1 = 0, \quad \dot{\theta}_2 = 0, \\ \ddot{\phi} &= 0, \quad \ddot{e}_x = 0, \quad \ddot{\theta}_1 = 0, \quad \ddot{\theta}_2 = 0. \end{aligned} \quad (69)$$

From Eqs.(45)-(47), it can be easily concluded that:

$$\dot{\phi} = 0\dot{x} = 0\ddot{\phi} = 0\ddot{x} = 0 \quad (70)$$

Combining Eqs.(2), (3), (6), (7), (69), and (70), the following results are obtained:

$$u_\phi = 0, \quad u_x = 0. \quad (71)$$

Considering the explicit expressions of u_ϕ and u_x in Eqs.(53), combining with Eqs.(47) and (69)-(71), it is easy to obtain that

$$e_\phi = 0e_x = 0. \quad (72)$$

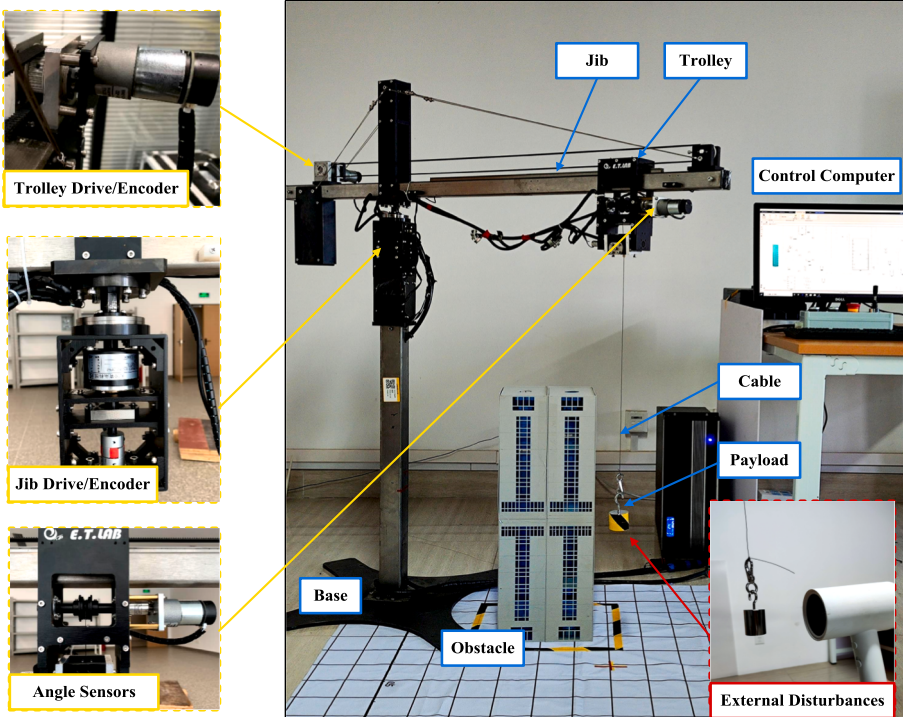


Fig. 5. Experimental equipment.

Substituting Eqs.(69)-(70) into Eqs.(4)-(5), one further has

$$mgl\theta_1 = 0 \quad mgl\theta_2 = 0. \quad (73)$$

Then, one can conclude that

$$\theta_1 = 0\theta_2 = 0. \quad (74)$$

As evident from Eqs.(72) and (74), it is demonstrated that all equilibrium points of the system reside within the largest invariant set Ω . Consequently, by employing LaSalle's invariance theorem, the result can be concluded that the error signals and the swing angles asymptotically converge to zero, i.e.,

$$\lim_{t \rightarrow \infty} e_\phi \rightarrow 0 \lim_{t \rightarrow \infty} e_x \rightarrow 0 \lim_{t \rightarrow \infty} \theta_1 \rightarrow 0 \lim_{t \rightarrow \infty} \theta_2 \rightarrow 0 \quad (75)$$

5. Experiment results

As shown in Fig. 5, the experimental platform is divided into: the measurement encoder section, the motor drive section, and the RT-DAC/PCI multi-function digital I/O board-equipped PC section. The control input signals are calculated in the MATLAB/Simulink Real-Time Windows Target. Then, the signals return to the drivers and generate the required control forces acting on the trolley and the jib.

The values of system parameters and variables are defined in Table 4. Moreover, the time parameters can be obtained as $t_s = 3.44$ s and $t_f = 7.47$ s, with the help of the FNN. Through the obstacle position, at the moment t_s , the positions of the jib and the trolley can be solved as follows: $\phi(t_s) = 26.5$ deg and $x(t_s) = 0.37$ m.

5.1. Comparison experiments

In this group, other existing effective control methods including the CTP control method and the S-shaped trajectory tracked by the PD controller are selected as comparisons to verify the effectiveness of the proposed method. To verify the obstacle avoidance performance of the proposed controller, identical obstacle avoidance tasks are assigned to all three control methods. The proposed controller has control gains set as

$$k_{p\phi} = 17k_{d\phi} = 8k_{px} = 25k_{dx} = 20\lambda_1 = 0.45\lambda_2 = 0.5a = 0.15b = 0.1$$

$$\hat{\omega}_\phi(0) = \text{diag}(0, 0, 0, 0, 0, 0) \hat{\omega}_x(0) = \text{diag}(0.15, 0, 0, 0) \varepsilon_{0\phi} = 0.01 \varepsilon_{0x} = 0.01$$

$$\Lambda_1 = \text{diag}\{0.1, 0.1, 0.05, 0.05, 0.05, 0.05\}, \text{ and } \Lambda_2 = \text{diag}\{0.3, 0.3, 0.1, 0.03, 0.05, 0.05\}.$$

Since the comparative methods lack obstacle avoidance capability, the whole transportation process are divided into two stages: the first process targets the bottom right of the safe range, and the second process aims for the terminal position of the payload. But, the proposed controller does not need that. Therefore, the proposed controller can reach the target position more smoothly and quickly..

The CTP control method is expressed as [25]:

$$\ddot{\phi} = \begin{cases} \frac{2\pi(\phi(t_s) - \phi_0)}{t_s} \left[1 - \cos\left(\frac{2\pi}{t_s}t\right) \right] + k_\phi m l x(t_s) \dot{\theta}_2, & t \in [0, t_s) \\ k_\phi m l x(t_s) \dot{\theta}_2, & t \in [t_s, t^*) \\ \frac{2\pi(\phi_d - \phi(t_s))(t - t^*)}{t_s} \left[1 - \cos\left(2\pi\left(\frac{t - t^*}{t_s}\right)\right) \right] + k_\phi m l x_d \dot{\theta}_2, & t \in [t^*, t^* + t_s) \\ k_\phi m l x_d \dot{\theta}_2, & t \in [t^* + t_s, t_{end}] \end{cases} \quad (76)$$

Table 4

The values of parameters and variables

| Symbols | Value & Unit | Symbols | Value & Unit | Symbols | Value & Unit |
|------------|-------------------------|--------------------|-----------------------|--------------------|--------------|
| M | 2 kg | w | 0.26 m | ϕ_0 | 10 deg |
| m | 0.3 kg | h | 0.31 m | x_0 | 0.17 m |
| J | 6.8 kg · m ² | δ | 0.02 m | ϕ_d | 50 deg |
| g | 9.8 m/s ² | $v_{\phi\max}$ | 35 deg/s | x_d | 0.65 m |
| l | 0.8 m | $a_{\phi\max}$ | 30 deg/s ² | x_1 | 0.18 m |
| t_1 | 5 s | $v_{x\max}$ | 0.9 m/s | y_1 | 0.34 m |
| t_2 | 20 s | $a_{x\max}$ | 0.9 m/s ² | $k_{\theta 2\max}$ | 2 deg |
| ϵ | 0.001 | $k_{\theta 1\max}$ | 2 deg | -- | -- |

$$\ddot{x} = \begin{cases} \frac{2\pi(x(t_s) - x_0)}{t_s} \left[1 - \cos\left(\frac{2\pi}{t_s}t\right) \right] + k_x m l \dot{\theta}_1, & t \in [0, t_s) \\ k_x m l \dot{\theta}_1, & t \in [t_s, t^*) \\ \frac{2\pi(x_d - x(t_s))(t - t^*)}{t_s} \left[1 - \cos\left(2\pi\left(\frac{t - t^*}{t_s}\right)\right) \right] + k_x m l \dot{\theta}_1, & t \in [t^*, t^* + t_s) \\ k_x m l \dot{\theta}_1, & t \in [t^* + t_s, t_{end}] \end{cases} \quad (77)$$

wherein $t_s = 4.9$ s, $t^* = 5.2$ s, $k_\phi = 0.001$, and $k_x = 0.005$ by adjusting.

The S-shaped trajectory is designed as follows [12] and [23]:

$$\phi = \begin{cases} \frac{(\phi(t_s) - \phi_0)}{2\pi} \left[\frac{2\pi t}{t_s} - \sin\left(\frac{2\pi t}{t_s}\right) \right] + \phi_0, & t \in [0, t_s) \\ \phi(t_s), & t \in [t_s, t^*) \\ \frac{(\phi_d - \phi(t_s))}{2\pi} \left[\frac{2\pi(t - t^*)}{t_s} - \sin\left(\frac{2\pi(t - t^*)}{t_s}\right) \right] + \phi(t_s), & t \in [t^*, t^* + t_s) \\ \phi_d, & t \in [t^* + t_s, t_{end}] \end{cases} \quad (78)$$

$$x = \begin{cases} \frac{(x(t_s) - x_0)}{2\pi} \left[\frac{2\pi t}{t_s} - \sin\left(\frac{2\pi t}{t_s}\right) \right] + x_0, & t \in [0, t_s) \\ x(t_s), & t \in [t_s, t^*) \\ \frac{(x_d - x(t_s))}{2\pi} \left[\frac{2\pi(t - t^*)}{t_s} - \sin\left(\frac{2\pi(t - t^*)}{t_s}\right) \right] + x(t_s), & t \in [t^*, t^* + t_s) \\ x_d, & t \in [t^* + t_s, t_{end}] \end{cases} \quad (79)$$

wherein $t_s = 4.8$ s and $t^* = 5.1$ s by adjusting. The PD controller's parameters i.e., $k_{p\phi}$, $k_{d\phi}$, k_{px} , and k_{dx} , are similar to the proposed controller.

Experimental results for this group are illustrated in Figs. 6–8. The parameters estimation result of the proposed controller is presented in Fig. 6, which clearly indicates that all the estimations converge within approximately 5 s for the proposed controller. And, from Fig. 7, it can be concluded that all three controllers respond promptly and ultimately eliminate the payload swing. However, the

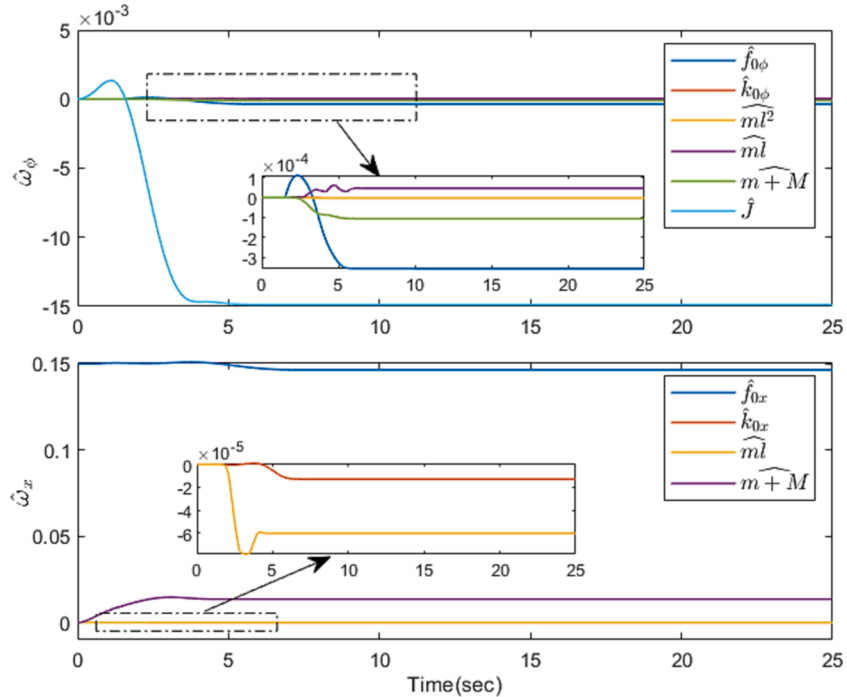


Fig. 6. The parameters estimation of the proposed controller.

proposed method achieves convergence 2.5 s faster than the others. Moreover, the proposed controller constrains the payload swings within smaller ranges compared to the other two controllers. By the proposed controller, the swing angle θ_1 stabilizes at 7.7 s, while the swing angle θ_2 stabilizes at 7.8 s. The proposed controller eliminates the payload swing angle more rapidly.

To illustrate the transportation process of the payload, Fig. 8 depicts the trajectory with an obstacle. Fig. 8 demonstrates that the proposed method successfully avoids obstacle collisions during transportation. Additionally, the obstacle avoidance trajectory of the proposed controller is smoother and faster than other control methods. In contrast, the comparative methods exhibit instability and extend into the safe range of obstacle avoidance.

5.2. Robustness Verification

This section will validate the robustness of the proposed method in three aspects. In the first part, the terminal position and obstacle position are changed. The second part of this experiment is validated by different payload masses. Finally, external disturbances are added to the system. In this section, the control gains/coefficients align with the values in Experiment 5.1.

Case 1: Robustness to random of the terminal position andm the obstacle position (as shown in Figs. 9–11)

The terminal position and the obstacle position are varied to verify the robustness of the proposed method in this group. The target positions are changed to $\phi_d = 47 \text{ deg}$ and $x_d = 0.6 \text{ m}$. The obstacles are arranged at different positions $x_1 = 0.16 \text{ m}$ and $y_1 = 0.32 \text{ m}$.

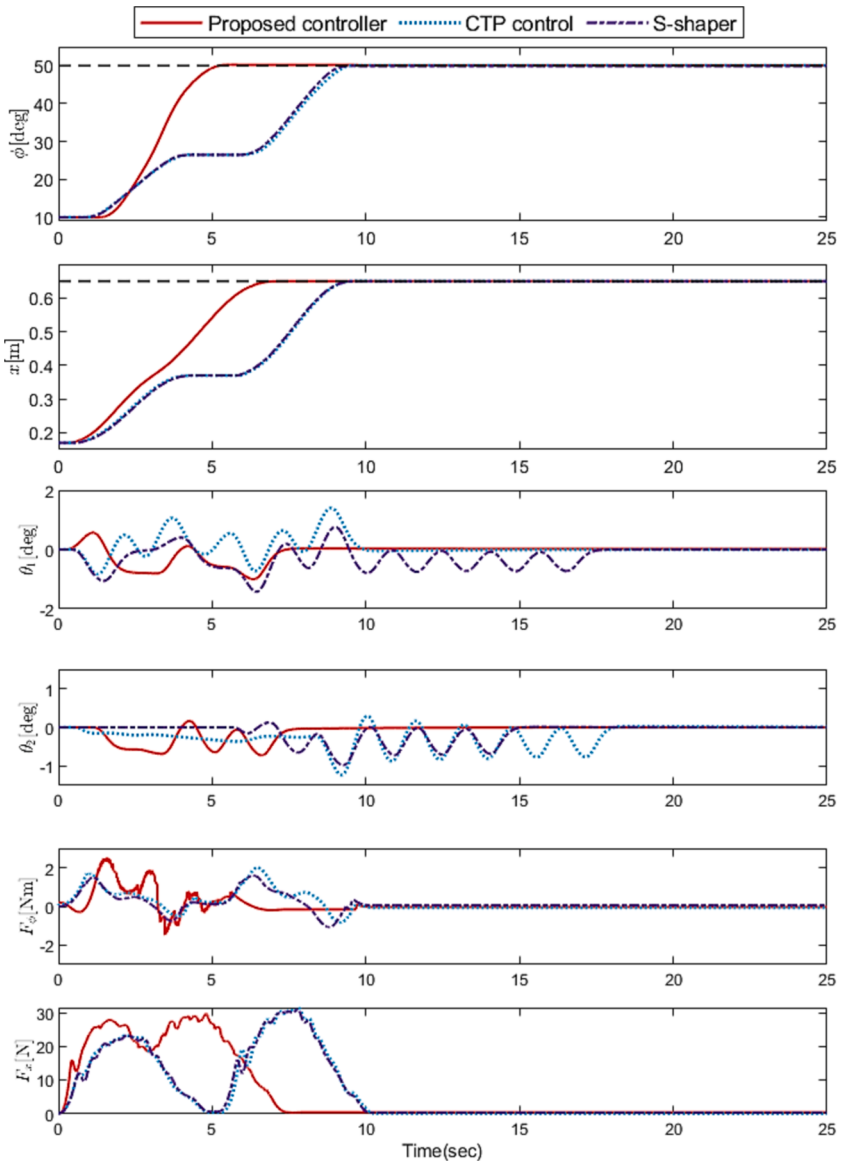


Fig. 7. The comparative experimental results.

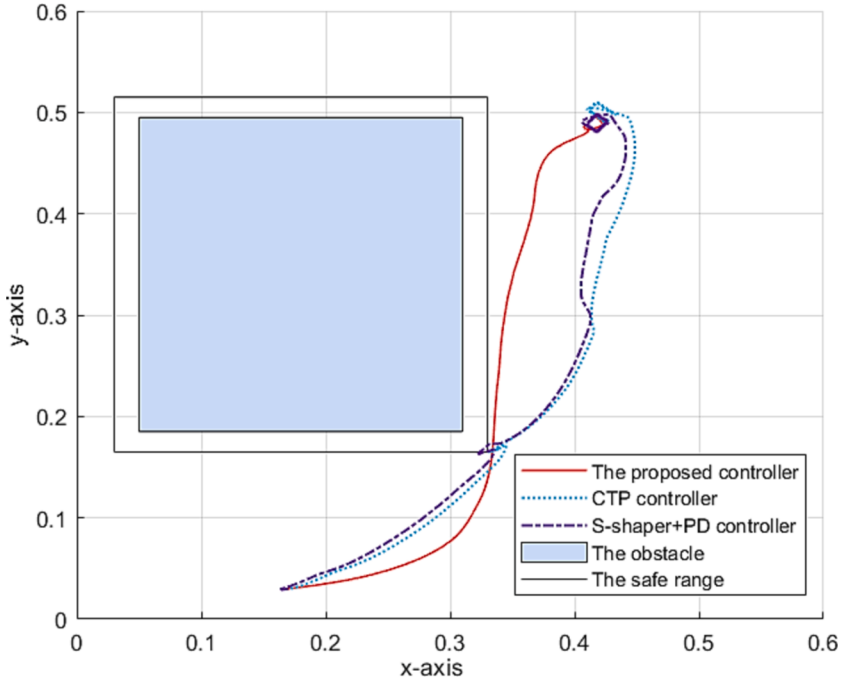


Fig. 8. The payload trajectory with the obstacle.

Utilizing the FNN, the proposed controller can determine the time parameters $t_s = 3.15$ s and $t_f = 6.96$ s. By calculation, $\phi(t_s) = 25$ deg and $x(t_s) = 0.34$ m in this group.

Case 2: Robustness to the uncertainty of the payload mass (as shown in Figs. 12–14)

This set of experiments changes the payload mass to $m = 0.4$ kg, to testify the control ability in dealing with parametric uncertainties. The time to encounter an obstacle is determined by the trolley coordinates, so the time parameters of the obstacle

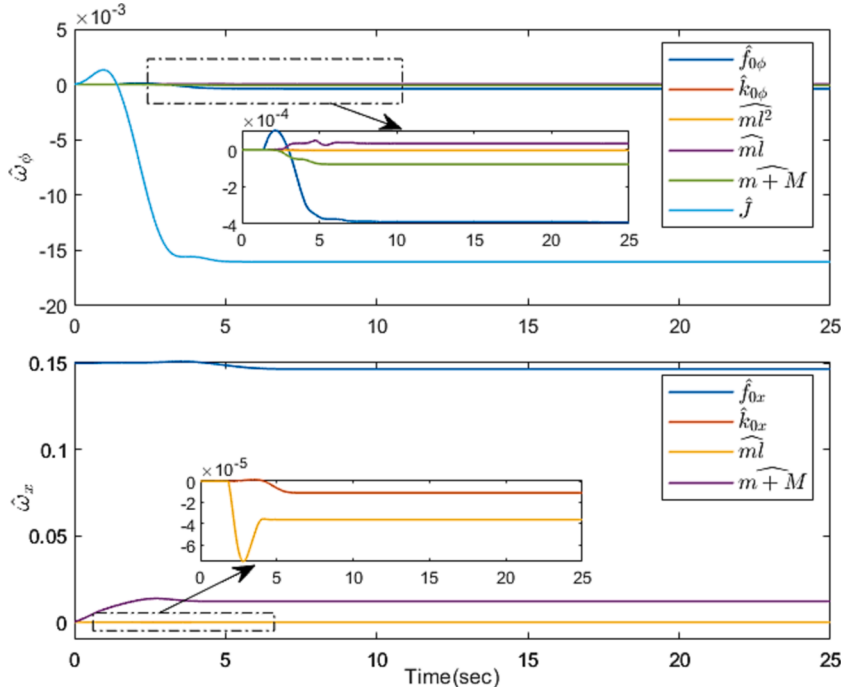


Fig. 9. Case 1: The parameters estimation of the proposed controller.

avoidance trajectory remain constant even when the mass of the payload changes.

Case 3: Robustness to persistent external disturbances (as shown in Figs. 15–17)

This section aims to test the robustness of control methods against initial system swing angles. The initial payload swings are added to the proposed controller, along with comparative control methods (the disturbances are manually introduced using a hairdryer).

5.3. Experimental results analysis

Figs. 9–17 illustrate the experimental results under the three conditions mentioned above. The corresponding experimental results demonstrate the robustness and effectiveness of the proposed controller.

Comparing Fig. 7 (solid red line) with Fig. 10, it can be concluded that there is a very small difference between the experimental results. This indicates that the proposed method has satisfactory performance for different system parameters. Despite variations in expected positions and obstacle positions, the proposed approach still has strong robustness. The proposed approach can still achieve control objectives successfully. The parameter estimations of the proposed controller are shown in Figs. 9, 12, 15, which clearly demonstrate that all parameter estimations converge in about 5 s for the three cases.

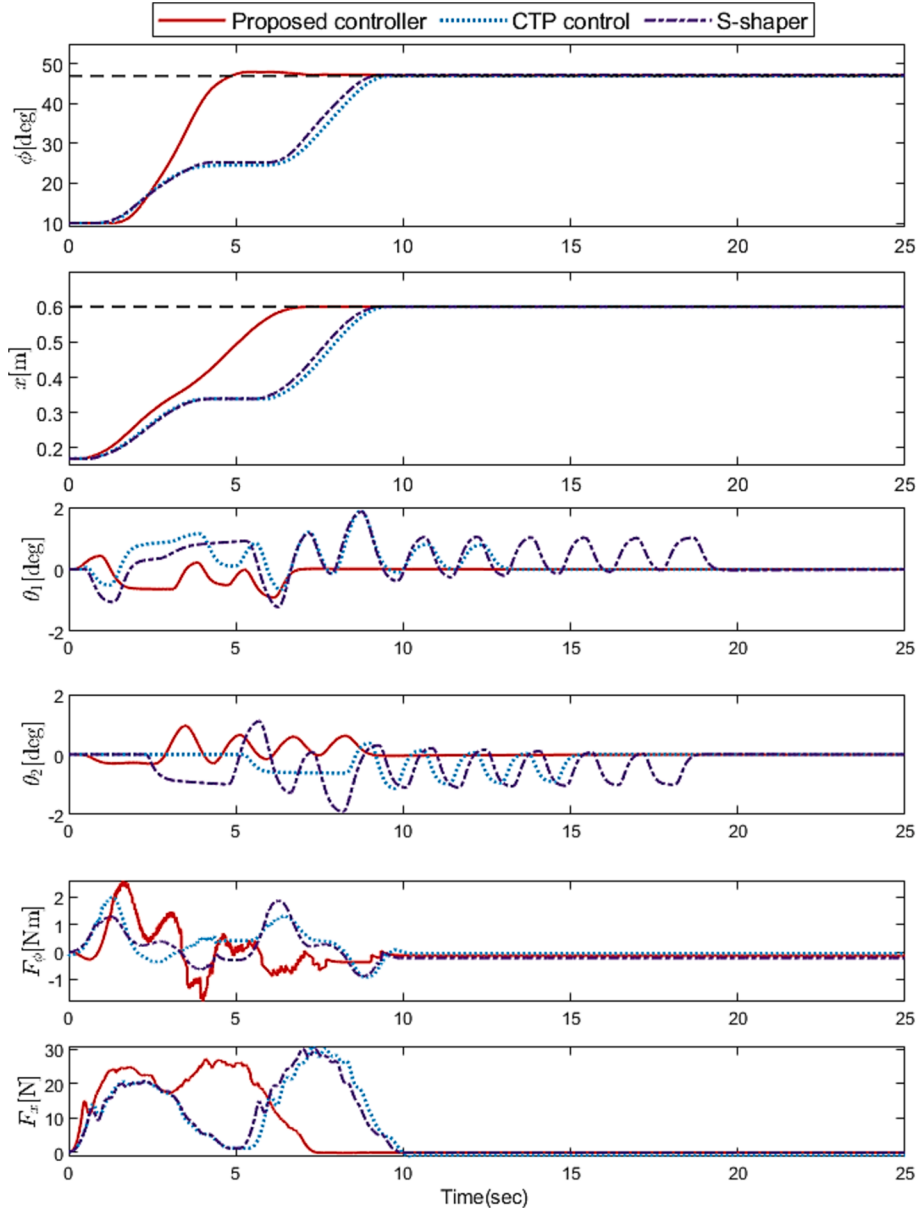


Fig. 10. Case 1: The comparative experimental results.

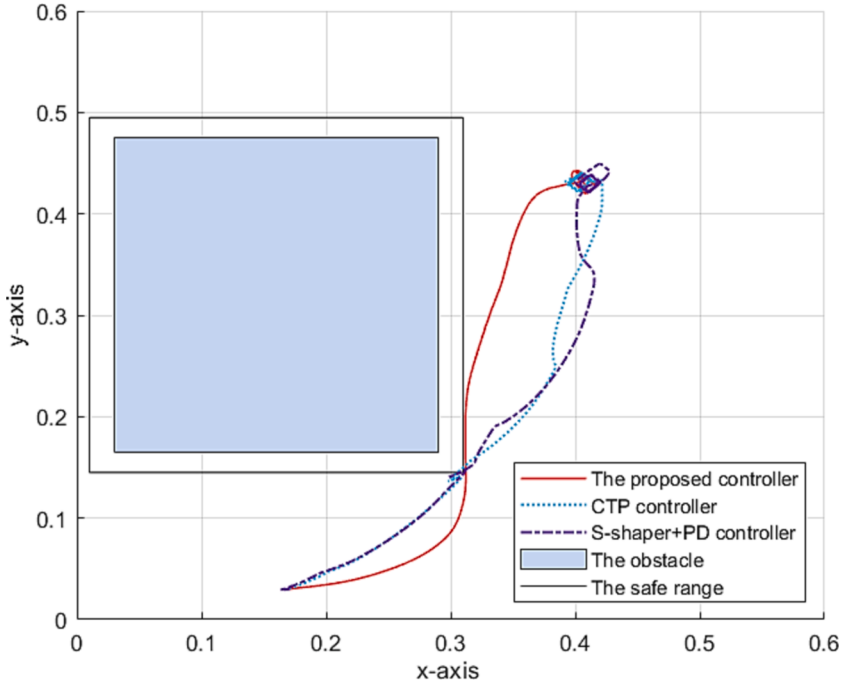


Fig. 11. Case 1: The payload trajectory with the obstacle.

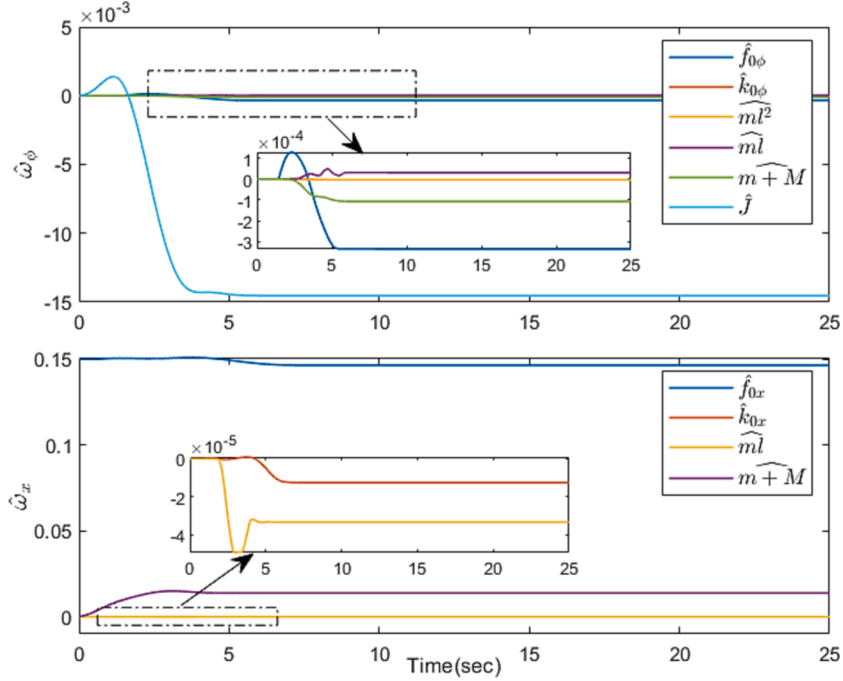


Fig. 12. Case 2: The parameters estimation of the proposed controller.

From Fig. 13, it can be observed that even when the payload mass is changed, the presented controller can still accomplish the control objective successfully. During transportation, the system maintains smooth swings, eliminates residual swing angles rapidly, and controls payload swing angles within 1 deg. Therefore, the proposed method exhibits strong robustness in handling different payload masses.

As can be seen in Fig. 16, the proposed control method can accurate positioning and quickly suppress the nonzero initial swing

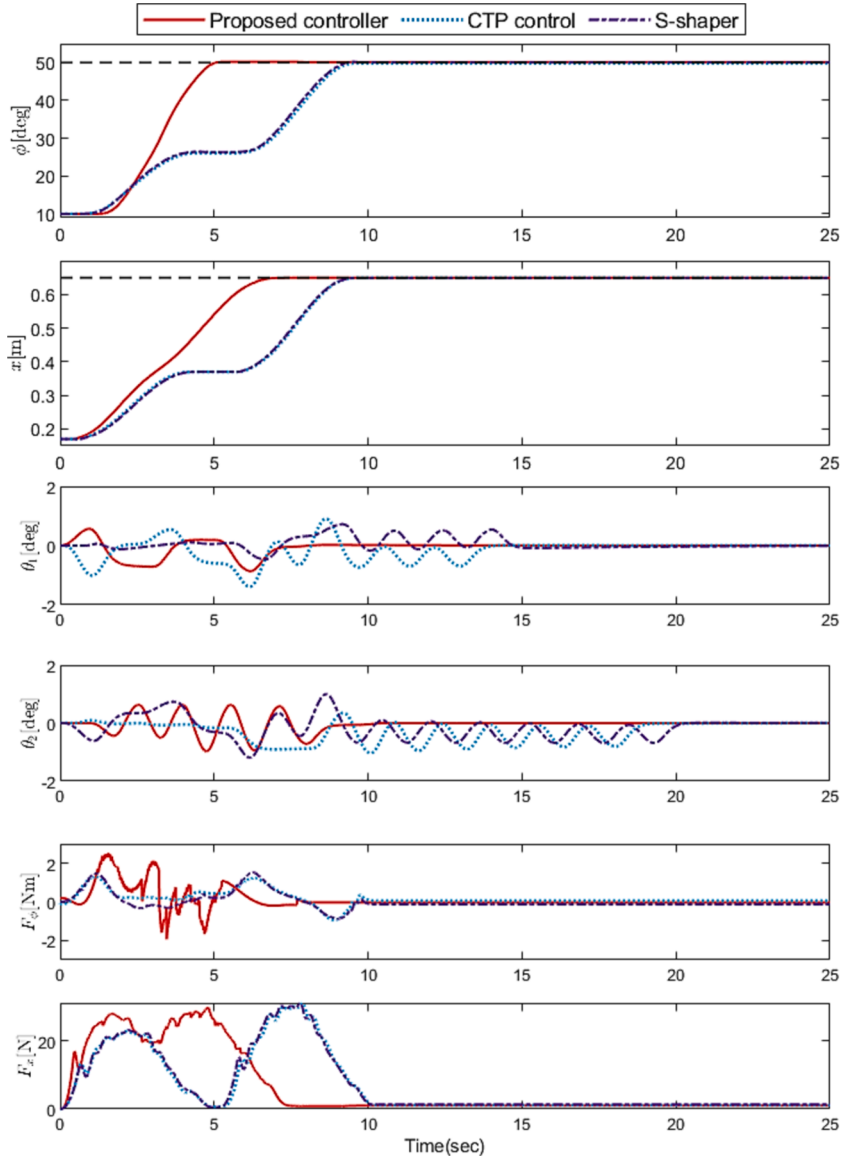


Fig. 13. Case 2: The comparative experimental results.

angles. The presented method can effectively eliminate unexpected external interference within 11.5 s, which is faster than the others. The other methods stabilize the angle swings after 20 s. It can be seen that the nonzero initial swing angle does not significantly affect the control performance of the proposed controller.

Fig. 18 illustrates the tracking error curves under four different scenarios for the proposed controller. In four cases, the tracking errors remain within the preset constraint ranges, which validates that the proposed controller has excellent tracking performance under various conditions.

6. Conclusion

To tackle the obstacle avoidance problem, this paper designs an optimal trajectory and an adaptive controller for 4-DOF tower cranes. First, some auxiliary signals are designed elaborately to express the state variables. Then, an optimal problem is established considering a series of physical constraints. Based on the dichotomy method, the optimal problem can be solved, and then the proposed method can design the optimal trajectory through FNN. In particular, the tracking errors are limited within a prior set of boundary conditions. The control method is theoretically analyzed using the Lyapunov method and LaSalle's invariance theorem. Finally, several groups of experiments are carried out to prove the effectiveness of the proposed strategy. The results indicate that all three controllers respond promptly, ultimately eliminating payload swing, with the proposed method achieving desired position faster than the others.

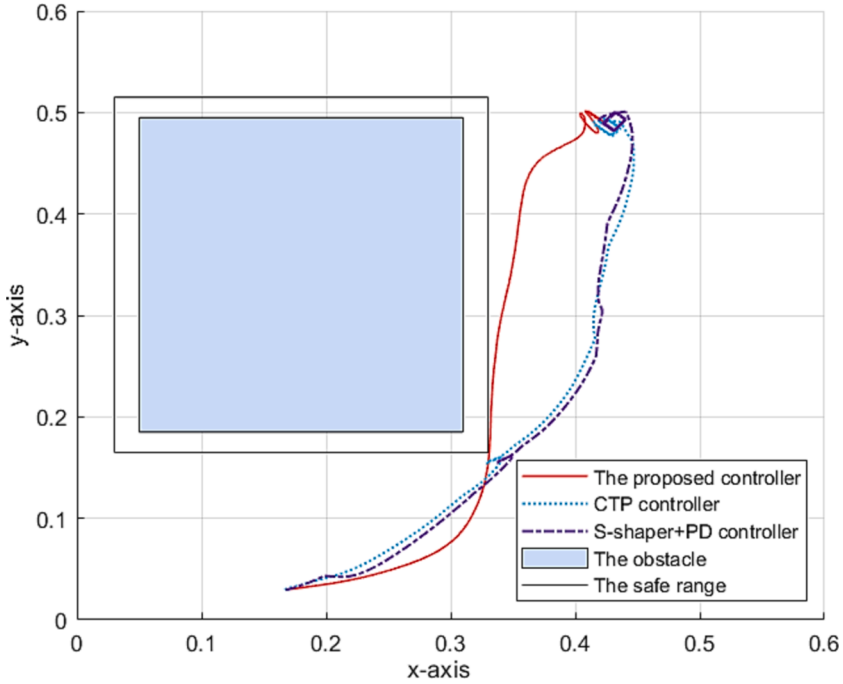


Fig. 14. Case 2: The payload trajectory with the obstacle.

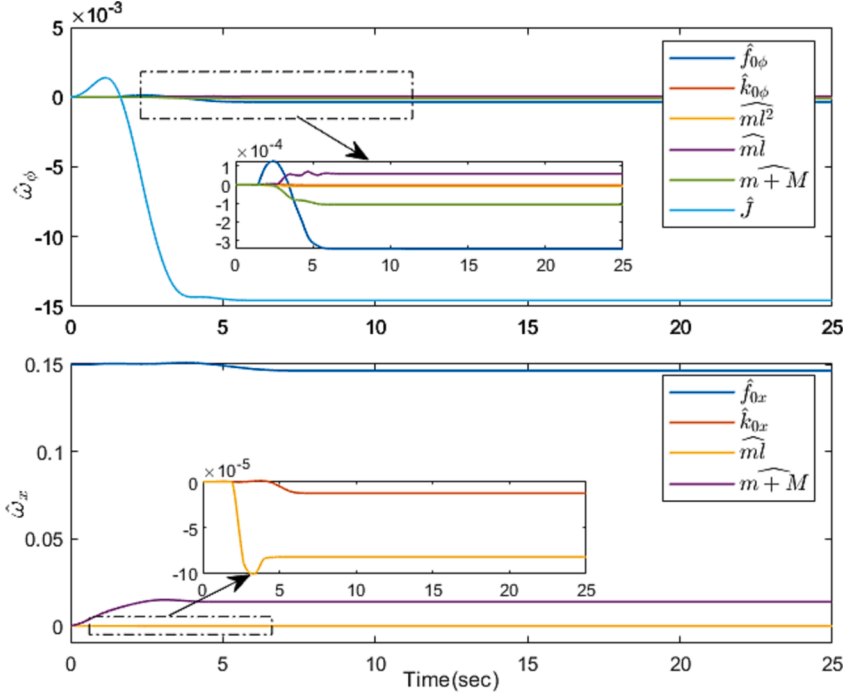


Fig. 15. Case 3: The parameters estimation of the proposed controller.

The proposed controller also constrains payload swings to smaller ranges, stabilizing the swing angle faster compared the others. In general, this innovative approach not only achieves precise positioning and swing suppression, but also avoids the obstacles in the movement path.

In the future, the current design will be extended to handle trajectory planning in environments with multiple obstacles. Additionally, we plan to expand the dataset to include more complex and diverse scenarios, allowing for more robust model training. Other

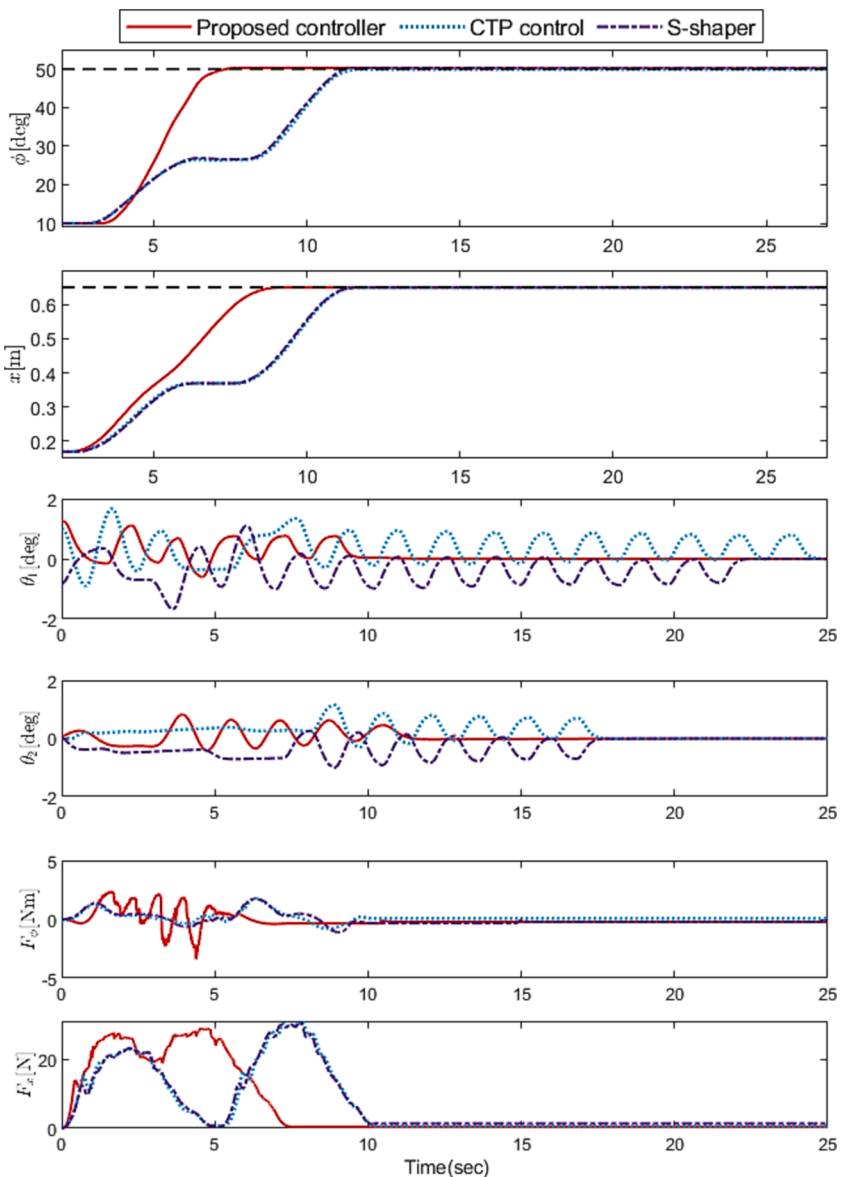


Fig. 16. Case 3: The comparative experimental results.

deep learning algorithms will be explored to improve the efficiency and accuracy of data processing in various environments.

CRediT authorship contribution statement

Wei Peng: Supervision, Funding acquisition, Conceptualization. **Hui Guo:** Writing – original draft, Validation, Data curation. **Menghua Zhang:** Methodology, Formal analysis. **Chengdong Li:** Project administration, Investigation. **Fang Shang:** Visualization, Software. **Zhi Li:** Validation.

Declaration of competing interest

The authors declare that they have no known competing financial interests or personal relationships that could have appeared to influence the work reported in this paper.

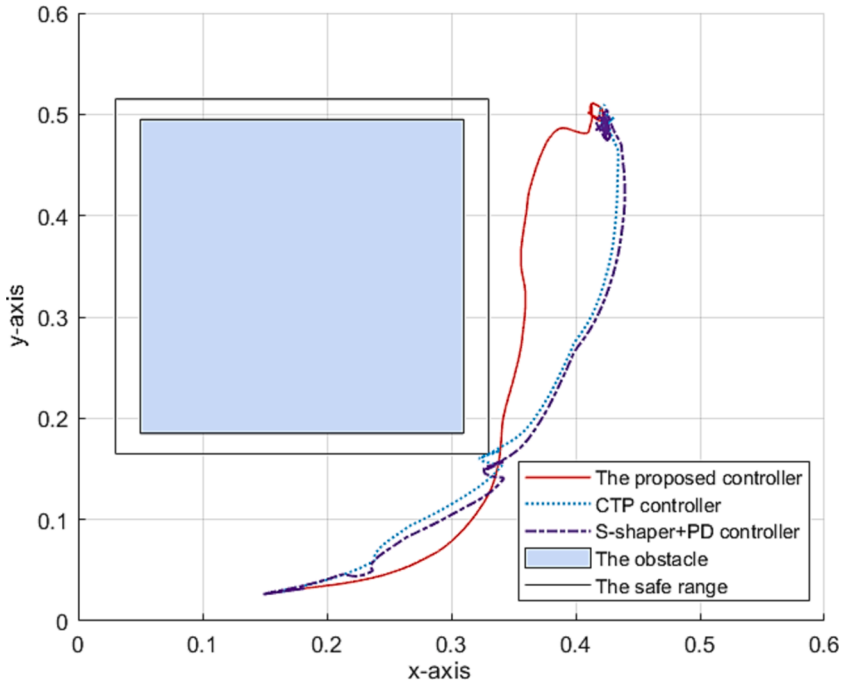


Fig. 17. Case 3: The payload trajectory with the obstacle.

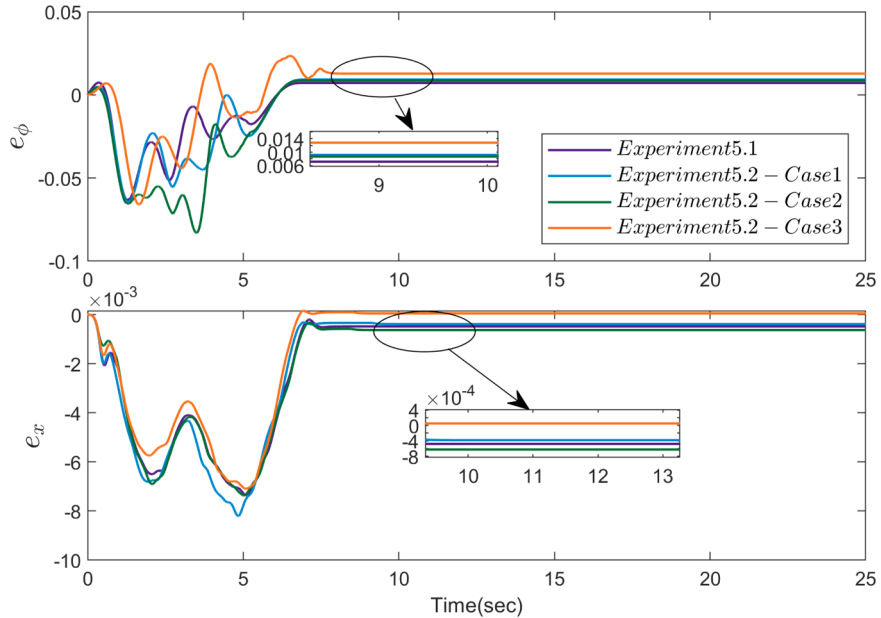


Fig. 18. The error curves of the proposed controller in four cases.

Acknowledgments

This work was supported in part by the National Natural Science Foundation of China under Grant No. 62273163, No. 61903226, No. 62076150, and No. 62173216, the Outstanding Youth Foundation of Shandong Province Under Grant No. ZR2023YQ056, the Key R&D Project of Shandong Province under Grant No. 2022CXGC010503, No. 2021CXGC011205, Shandong Provincial Science, Technology SME Innovation Capability Improving Project No. 2022TSGC2157, and the Taishan Scholars Program.

Appendix A

Training data collection for FNN.

| Num. | x_d | ϕ_d | x_1 | y_1 | t_f | t_s | Num. | x_d | ϕ_d | x_1 | y_1 | t_f | t_s |
|------|-------|----------|-------|-------|--------|--------|------|-------|----------|-------|-------|--------|--------|
| 1 | 0.5 | 45 | 0.2 | 0.32 | 6.5134 | 3.6584 | 21 | 0.65 | 47 | 0.07 | 0.34 | 7.5607 | 2.7311 |
| 2 | 0.52 | 45 | 0.2 | 0.32 | 6.6763 | 3.6357 | 22 | 0.65 | 47 | 0.09 | 0.34 | 7.5607 | 2.8751 |
| 3 | 0.54 | 45 | 0.2 | 0.32 | 6.8320 | 3.6180 | 23 | 0.65 | 47 | 0.11 | 0.34 | 7.5607 | 3.0148 |
| 4 | 0.56 | 45 | 0.2 | 0.32 | 6.9785 | 3.6026 | 24 | 0.65 | 47 | 0.13 | 0.34 | 7.5607 | 3.1512 |
| 5 | 0.58 | 45 | 0.2 | 0.32 | 7.1194 | 3.5903 | 25 | 0.65 | 47 | 0.15 | 0.34 | 7.5607 | 3.2850 |
| 6 | 0.6 | 45 | 0.2 | 0.32 | 7.2549 | 3.5800 | 26 | 0.65 | 47 | 0.17 | 0.34 | 7.5607 | 3.4172 |
| 7 | 0.62 | 45 | 0.2 | 0.32 | 7.3849 | 3.5712 | 27 | 0.65 | 47 | 0.19 | 0.34 | 7.5607 | 3.5485 |
| 8 | 0.64 | 45 | 0.2 | 0.32 | 7.5095 | 3.5632 | 28 | 0.65 | 47 | 0.21 | 0.34 | 7.5607 | 3.6796 |
| 9 | 0.66 | 45 | 0.2 | 0.32 | 7.6285 | 3.5558 | 29 | 0.65 | 47 | 0.23 | 0.34 | 7.5607 | 3.8112 |
| 10 | 0.68 | 45 | 0.2 | 0.32 | 7.7438 | 3.5493 | 30 | 0.65 | 47 | 0.25 | 0.34 | 7.5607 | 3.9441 |
| 11 | 0.6 | 46 | 0.22 | 0.3 | 7.2513 | 3.6684 | 31 | 0.65 | 47 | 0.16 | 0.2 | 7.5607 | 3.0398 |
| 12 | 0.6 | 47 | 0.22 | 0.3 | 7.2476 | 3.6665 | 32 | 0.65 | 47 | 0.16 | 0.22 | 7.5607 | 3.0579 |
| 13 | 0.6 | 48 | 0.22 | 0.3 | 7.2421 | 3.6638 | 33 | 0.65 | 47 | 0.16 | 0.24 | 7.5607 | 3.0859 |
| 14 | 0.6 | 49 | 0.22 | 0.3 | 7.2385 | 3.6619 | 34 | 0.65 | 47 | 0.16 | 0.26 | 7.5607 | 3.1232 |
| 15 | 0.6 | 50 | 0.22 | 0.3 | 7.2348 | 3.6601 | 35 | 0.65 | 47 | 0.16 | 0.28 | 7.5607 | 3.1691 |
| 16 | 0.6 | 51 | 0.22 | 0.3 | 7.2293 | 3.6573 | 36 | 0.65 | 47 | 0.16 | 0.3 | 7.5607 | 3.2230 |
| 17 | 0.6 | 52 | 0.22 | 0.3 | 7.2256 | 3.6554 | 37 | 0.65 | 47 | 0.16 | 0.32 | 7.5607 | 3.2839 |
| 18 | 0.6 | 53 | 0.22 | 0.3 | 7.2202 | 3.6526 | 38 | 0.65 | 47 | 0.16 | 0.34 | 7.5607 | 3.3513 |
| 19 | 0.6 | 54 | 0.22 | 0.3 | 7.2165 | 3.6508 | 39 | 0.65 | 47 | 0.16 | 0.36 | 7.5607 | 3.4244 |
| 20 | 0.6 | 55 | 0.22 | 0.3 | 7.2110 | 3.6480 | 40 | 0.65 | 47 | 0.16 | 0.38 | 7.5607 | 3.5027 |

Appendix B

The coefficients of t_f are:

$$a_{ij} = \begin{bmatrix} [1.197173541.36446151 - 1.628798411.07378936] \\ [1.36889391.14661601 - 1.812884061.98628404] \\ [0.770796430.30500349 - 1.94386927 - 0.15568974] \\ [1.866894420.96948444 - 0.4221005 - 1.07603338] \end{bmatrix}$$

$$b_{ij} = \begin{bmatrix} [0.90956569 - 0.285172 - 1.04586551 - 1.40619032] \\ [-0.39824895 - 1.74657418 - 0.046452641.09671144] \\ [1.26169546 - 0.61542403 - 0.464601450.65493194] \\ [1.36287124 - 0.327839180.06797926 - 1.54968994] \end{bmatrix}$$

$$w_m = [1.69334934e + 005.49329765e - 018.64327590e - 011.27367915e + 009.98745205e - 011.15412480e + 004.78978502e - 011.11713808e + 005.76363544e - 014.45191878e - 011.97910107e + 001.48431125e + 001.07220497e + 001.58320427e + 001.34473127e + 001.61962416e + 002.43193123e + 008.38280444e - 011.45320827e + 002.02246884e + 004.73104085e - 011.00046790e + 009.03819422e - 011.74152987e + 001.91743554e + 001.39202899e + 005.06042653e - 015.14074525e - 011.42623737e + 002.27058734e - 011.68571801e + 001.18848723e + 003.14877563e - 011.96547797e + 001.88045135e + 008.95148068e - 011.97176103e + 007.58016677e - 011.71267392e + 006.25608943e - 011.17655573e + 001.33067910e + 001.192555399e + 007.62588308e - 012.78221919e - 019.65051910e - 011.07061314e + 001.33290571e - 011.61309003e - 027.86828167e - 011.86955173e + 001.67446154e + 002.44506190e - 015.77815360e - 011.81107783e + 002.73016038e - 014.54783016e - 011.38104313e + 001.18692256e + 009.67711520e - 011.562841005e - 012.62145371e - 012.68297923e - 014.10734818e - 011.88552403e + 003.75437212e - 011.885373077e - 019.40025804e - 012.07972466e - 012.04359330e - 011.36952447e + 008.69583414e - 011.99410558e + 001.44146112e + 008.27001784e - 015.33152966e - 011.52331673e + 001.90405160e + 001.21283781e + 001.28873327e + 001.44335503e + 001.72849355e + 001.47820544e + 005.10742032e - 011.31912704e - 021.17713014e - 017.30546435e - 015.11088481e - 011.59558400e + 001.38902620e + 001.61866712e + 001.48737772e + 001.35592426e + 007.55912390e - 016.46732443e - 011.81345901e + 005.11955432e - 011.82050384e + 001.04354719e + 001.20843621e - 019.69049748e - 019.27801854e - 022.80511138e - 011.52812873e + 001.15382423e - 011.21127378e - 011.32534825e + 001.85407260e + 001.19059880e + 003.81724677e - 011.88308361e + 001.83025886e + 007.31466846e - 018.05097857e - 01]$$

The coefficients of t_s are:

$$a_{ij} = \begin{bmatrix} [-1.8963831 - 0.392443471.92828088 - 1.09517026] \\ [0.30215853 - 0.753526680.65080654 - 1.90038299] \\ [-1.54729131 - 1.75195829 - 0.4176461 - 0.41566936] \\ [-0.874699050.24677697 - 1.52204845 - 0.9844266] \end{bmatrix}$$

$$b_{ij} = \begin{bmatrix} [-1.83918734 - 1.22946961.12289785 - 1.56957904] \\ [-0.46465228 - 0.50276823 - 0.850902481.32010052] \\ [0.78383961 - 0.1862546 - 0.36647333 - 1.29637017] \\ [-0.962286530.131897091.64330207 - 0.88809536] \end{bmatrix}$$

$$\begin{aligned} w_m = & [1.69334934e + 005.49329765e - 018.64327590e - 011.27367915e + 009.98745205e - 011.15412480e + 00 \\ & 4.78978502e - 011.11713808e + 005.76363544e - 014.45191878e - 011.97910107e + 001.48431125e + 00 \\ & 1.07220497e + 001.58320427e + 001.34473127e + 001.61962416e + 002.43193123e + 008.38280444e - 01 \\ & -1.45320827e + 002.02246884e + 004.73104085e - 011.00046790e + 009.03819422e - 011.74152987e + 00 \\ & 1.91743554e + 001.39202899e + 005.06042653e - 015.14074525e - 011.42623737e + 002.27058734e - 01 \\ & 1.68571801e + 001.18848723e + 003.14877563e - 011.96547797e + 001.88045135e + 008.95148068e - 01 \\ & 1.97176103e + 007.58016677e - 011.71267392e + 006.25608943e - 011.17655573e + 001.33067910e + 00 \\ & 1.92555399e + 007.62588308e - 012.78221919e - 019.65051910e - 011.07061314e + 001.33290571e - 01 \\ & 1.61309003e - 027.86828167e - 011.86955173e + 001.67446154e + 002.44506190e - 015.77815360e - 01 \\ & 1.81107783e + 002.73016038e - 014.54783016e - 011.38104313e + 001.18692256e + 009.67711520e - 01 \\ & 5.62841005e - 012.62145371e - 012.68297923e - 014.10734818e - 011.88552403e + 003.75437212e - 01 \\ & 8.85373077e - 019.40025804e - 012.07972466e - 012.04359330e - 011.36952447e + 008.69583414e - 01 \\ & 1.99410558e + 001.44146112e + 008.27001784e - 015.33152966e - 011.52331673e + 001.90405160e + 00 \\ & 1.21283781e + 001.28873327e + 001.44335503e + 001.72849355e + 001.47820544e + 005.10742032e - 01 \\ & 1.31912704e - 021.17713014e - 017.30546435e - 015.11088481e - 011.59558400e + 001.38902620e + 00 \\ & 1.61866712e + 001.48737772e + 001.35592426e + 007.55912390e - 016.46732443e - 011.81345901e + 00 \\ & 5.11955432e - 011.82050384e + 001.04354719e + 001.20843621e - 019.69049748e - 019.27801854e - 02 \\ & 2.80511138e - 011.52812873e + 001.15382423e - 011.21127378e - 011.32534825e + 001.85407260e + 00 \\ & 1.19059880e + 003.81724677e - 011.88308361e + 001.83025886e + 007.31466846e - 018.05097857e - 01] \end{aligned}$$

Data availability

Data will be made available on request.

References

- [1] M. Zhang, X. Jing, Z. Zhu, Disturbance employment-based sliding mode control for 4-DOF tower crane systems, *Mech. Syst. Signal Process.* 161 (2021) 107946, <https://doi.org/10.1016/j.ymssp.2021.107946>.
- [2] T. Yang, N. Sun, H. Chen, Y. Fang, Observer-based nonlinear control for tower cranes suffering from uncertain friction and actuator constraints with experimental verification, *IEEE Trans. Ind. Electron.* 68 (7) (2021) 6192–6204, <https://doi.org/10.1109/TIE.2020.2992972>.
- [3] M. Zhang, Y. Zhang, B. Ji, C. Ma, X. Cheng, Modeling and energy-based sway reduction control for tower crane systems with double-pendulum and spherical-pendulum effects, *Meas. Control* 53 (1–2) (2020) 141–150, <https://doi.org/10.1177/0020294019877492>.
- [4] M. Zhang, X. Jing, Model-free saturated PD-SMC method for 4-DOF tower crane systems, *IEEE Trans. Ind. Electron.* 69 (10) (2022) 10270–10280, <https://doi.org/10.1109/TIE.2021.3139134>.
- [5] M. Zhai, N. Sun, T. Yang, Y. Fang, Underactuated mechanical systems with both actuator and actuated/unactuated state constraints: a predictive control-based approach, *IEEE/ASME Trans. Mechatron.* 28 (3) (2023) 1359–1371, <https://doi.org/10.1109/TMECH.2022.3230244>.
- [6] M. Zhang, Y. Zhang, B. Ji, C. Ma, X. Cheng, Adaptive sway reduction for tower crane systems with varying cable lengths, *Autom. Constr.* 119 (2020) 103342, <https://doi.org/10.1016/j.autcon.2020.103342>.
- [7] Y. Wu, N. Sun, H. Chen, Y. Fang, Adaptive output feedback control for 5-DOF varying-cable-length tower cranes with cargo mass estimation, *IEEE Trans. Ind. Inform.* 17 (4) (2021) 2453–2464, <https://doi.org/10.1109/TII.2020.3006179>.
- [8] H. Ouyang, Z. Tian, L. Yu, G. Zhang, Adaptive tracking controller design for double-pendulum tower cranes, *Mech. Mach. Theory* 153 (2020) 103980, <https://doi.org/10.1016/j.mechmactheory.2020.103980>.
- [9] P. Van Trieu, H.M. Cuong, H.Q. Dong, N.H. Tuan, Adaptive fractional-order fast terminal sliding mode with fault-tolerant control for underactuated mechanical systems: Application to tower cranes, *Autom. Constr.* 123 (2021) 103533, <https://doi.org/10.1016/j.autcon.2020.103533>.
- [10] Z. Liu, N. Sun, Y. Wu, X. Xin, Y. Fang, Nonlinear sliding mode tracking control of underactuated tower cranes, *Int. J. Control Autom. Syst.* 19 (2) (2021) 1065–1077, <https://doi.org/10.1007/s12555-020-0033-5>.
- [11] M. Zhang, Y. Zhang, H. Ouyang, C. Ma, X. Cheng, Adaptive integral sliding mode control with payload sway reduction for 4-DOF tower crane systems, *Nonlinear Dyn.* 99 (4) (2020) 2727–2741, <https://doi.org/10.1007/s11071-020-05471-3>.
- [12] Z. Sun, H. Ouyang, Adaptive fuzzy tracking control for vibration suppression of tower crane with distributed payload mass, *Autom. Constr.* 142 (2022) 104521, <https://doi.org/10.1016/j.autcon.2022.104521>.
- [13] T. Yang, N. Sun, Y. Fang, Adaptive fuzzy control for a class of MIMO underactuated systems with plant uncertainties and actuator deadzones: design and experiments, *IEEE Trans. Cybern.* 52 (8) (2022) 8213–8226, <https://doi.org/10.1109/TCYB.2021.3050475>.
- [14] M. Zhang, X. Jing, Z. Zhou, W. Huang, Transportation for 4-DOF tower cranes: a periodic sliding mode control approach, *IEEE Trans. Intell. Transport. Syst.* (2024) 1–13, <https://doi.org/10.1109/TITS.2024.3412158>.
- [15] J. Xia, H. Ouyang, M. Zhang, Fault-tolerant controller design based on adaptive backstepping for tower cranes with actuator faults, *ISA Trans.* 146 (2024) 463–471, <https://doi.org/10.1016/j.isatra.2023.12.032>.

- [16] J. Xia, H. Ouyang, S. Li, Fixed-time observer-based back-stepping controller design for tower cranes with mismatched disturbance, *Nonlinear Dyn.* 111 (1) (2023) 355–367, <https://doi.org/10.1007/s11071-022-07851-3>.
- [17] M. Zhang, X. Jing, Adaptive neural network tracking control for double-pendulum tower crane systems with nonideal inputs, *IEEE Trans. Syst. Man Cybern. Syst.* 52 (4) (2022) 2514–2530, <https://doi.org/10.1109/TSMC.2020.3048722>.
- [18] S. M. F. ur Rehman *et al.*, “Adaptive input shaper for payload swing control of a 5-DOF tower crane with parameter uncertainties and obstacle avoidance,” *Autom. Constr.*, vol. 154, p. 104963, Oct. 2023, doi: 10.1016/j.autcon.2023.104963.
- [19] H. Chen, N. Sun, Nonlinear control of underactuated systems subject to both actuated and unactuated state constraints with experimental verification, *IEEE Trans. Ind. Electron.* 67 (9) (2020) 7702–7714, <https://doi.org/10.1109/TIE.2019.2946541>.
- [20] H. Chen, R. Zhang, W. Liu, H. Chen, A time optimal trajectory planning method for offshore cranes with ship roll motions, *J. Franklin. Inst.* 359 (12) (2022) 6099–6122, <https://doi.org/10.1016/j.jfranklin.2022.06.007>.
- [21] Z. Liu, N. Sun, Y. Wu, H. Chen, X. Liang, and Y. Fang, “Multi-objective trajectory planning with state constraints for 5-DOF underactuated tower crane systems,” *Advances in Applied Nonlinear Dynamics, Vibration and Control -2021*, vol. 799, X. Jing, H. Ding, and J. Wang, Eds., in Lecture Notes in Electrical Engineering, vol. 799, , Singapore: Springer Singapore, 2022, pp. 710–728. doi: 10.1007/978-981-16-5912-6_52.
- [22] W. Zhang, H. Chen, H. Chem, W. Liu, A time optimal trajectory planning method for double-pendulum crane systems with obstacle avoidance, *IEEE Access* 9 (2021) 13022–13030, <https://doi.org/10.1109/ACCESS.2021.3050258>.
- [23] H. Zhu, H. Ouyang, H. Xi, Neural network-based time optimal trajectory planning method for rotary cranes with obstacle avoidance, *Mech. Syst. Signal Process.* 185 (2023) 109777, <https://doi.org/10.1016/j.ymssp.2022.109777>.
- [24] H. Chen, Y. Fang, N. Sun, An adaptive tracking control method with swing suppression for 4-DOF tower crane systems, *Mech. Syst. Signal Process.* 123 (2019) 426–442, <https://doi.org/10.1016/j.ymssp.2018.11.018>.
- [25] H. Ouyang, Z. Tian, L. Yu, G. Zhang, Motion planning approach for payload swing reduction in tower cranes with double-pendulum effect, *J. Franklin. Inst.* 357 (13) (2020) 8299–8320, <https://doi.org/10.1016/j.jfranklin.2020.02.001>.
- [26] M. Zhang, X. Ma, X. Rong, X. Tian, Y. Li, Adaptive tracking control for double-pendulum overhead cranes subject to tracking error limitation, parametric uncertainties and external disturbances, *Mech. Syst. Signal Process.* 76–77 (2016) 15–32.